Secular variations in seawater chemistry controlling dolomitisation in shallow reflux systems: insights from reactive transport modelling

Tatyana Gabellone* (tatyana.gabellone@bristol.ac.uk) and Fiona Whitaker (Fiona.Whitaker@bristol.ac.uk)

School of Earth Sciences, University of Bristol, Wills Memorial Building, Queen's Road, Bristol, BS8 1RJ, UK

*corresponding author

Running title: RTM of reflux dolomitisation

(A) ABSTRACT

Dolomitisation often plays a critical role in the pore network development of platform carbonates, with implications for reservoir quality distribution. Understanding both the hydrological system driving dolomitisation and the chemistry of the fluids involved is fundamental to constrain predictions of the geometry and the petrophysical properties of dolomite bodies. Here the role of secular variations in seawater Mg/Ca as a control on dolomitisation and early porosity modification was evaluated using 1D Reactive Transport Models (RTM) and fluids based on modern (aragonite sea), Mississippian and Aptian (calcite sea) seawaters. The sensitivity of dolomitisation to a range of extrinsic controls (brine salinity, temperature, fluid flow rate, and pCO_2), and to intrinsic reactivity of the sediments (effective reactive surface area) was also explored. Simulations suggest faster calcite replacement by dolomite for seawaters with higher Mg/Ca, indicating dolomitisation potential is determined more by Mg/Ca rather than saturation index. Increasing evaporative concentration enhances reaction rate independent of the effect of enhanced density-driven fluid flux. In addition to brine composition, effective surface area of precursor sediments and temperature exert a critical control on replacement rate, whilst secular variations of pH and carbonate alkalinity associated with changes in pCO_2 are only secondary controls. Above flow rates of 0.01 m/yr replacive dolomitisation is reaction- rather than flux-limited, favouring alteration of fine-grained carbonates and suggesting that preferential alteration of grainstone units is rare unless head gradients are low. Post-replacement dolomite cementation is flux dependent, and thus favoured in areas of high head gradient and high permeability sediments, and, contrarily to replacement, supersaturation is a more important driver than Mg/Ca. Whilst uncertainties remain regarding low-temperature dolomitisation kinetics, the capability of numerical simulations to decouple individual controls provides new insights

which can be used, in conjunction with traditional comparative sedimentology, to generate more rigorous conceptual models for individual reservoir settings.

Keywords: dolomitisation, reactive transport modelling, reflux, seawater chemistry, Mg/Ca, secular fluctuations.

(A) INTRODUCTION

Characterization of the geometry of dolomite geobodies (and any associated dissolution, silicification, diagenetic evaporites and MVT deposits) and the resulting patterns of porosity and permeability is a key achievement both in reducing risk in resource assessment and optimising recovery. It is now widely accepted that the geometry and reservoir properties of the dolomite bodies depend on the hydrological system driving dolomitisation and also on the chemistry of the fluids (Morrow, 1982; Land, 1985; Warren, 2000; Machel, 2004).

Although dolomitising solutions can have multiple origins and compositions, there is a general agreement that seawater is the only abundant source of magnesium capable of causing massive dolomitisation (Land, 1985; Sun, 1994; Warren, 2000). Many of these dolomite reservoirs occur in subtidal carbonates associated with evaporitic tidal flat/lagoon environments and their origin appears to be related to reflux of fluids formed by solar-driven concentration of seawater (Adams & Rhodes, 1960; Fisher & Rodda, 1969; Montañez & Read, 1992; Sun, 1995; Rivers *et al*., 2012). Fluid flow is driven by the density contrast between the denser, evaporated seawater which develops over restricted areas of the platform top and the normal salinity seawater of the open areas of shelf and adjacent basin plus the interstitial pore water in the subtidal deposits underlying the evaporitic tidal flat/lagoonal deposits. There are also cases reporting dolomites formed by reflux of mesosaline brines and

not associated with the precipitation of evaporites, indicating that even a small density contrast may be enough to drive reflux (Simms, 1984; Whitaker & Smart, 1990; Melim & Scholle, 2002; Gabellone *et al*., 2014a).

Within reflux systems mole-for-mole replacement of calcite by dolomite tends to generate an initial increase in porosity in the updip direction close to the brine source (Saller & Henderson, 1998). This is commonly associated with a significant increase in permeability, especially when lime mudstones and wackestones are replaced with sucrosic dolomite crystals (Dawans & Swart, 1988; Woody *et al.*, 1996). However, continued flow of supersaturated fluids through the previously dolomitised rocks causes dolomite overgrowth and cementation of intercrystalline pores ("overdolomitisation"; Halley & Schmoker, 1983; Lucia, 2004) which may reduce permeability. On the other hand, the flow of undersaturated fluids, during either meteoric or burial diagenesis may be responsible for porosity increase in partially- to completely-dolomitised carbonates (Machel & Anderson, 1989; Mazzullo & Harris, 1992; Amthor *et al*., 1994; Wright & Harris, 2013). Reflux dolomitisation predicted to result in better reservoir properties in the more distal parts of the flow system where the brines become progressively less dolomite supersaturated (Lucia & Major, 1994; Saller *et al.*, 1994; Saller, 2004; Wahlman, 2010). However, this may be countered by porosity occluding evaporite precipitation which results from the release of calcium during replacement of calcite by dolomite in combination with the available sulphate in the brines (Machel, 1986; Leary & Vogt, 1987).

The geochemical potential for dolomitisation is strongly influenced by the Mg/Ca of the refluxing fluids, which reflects the chemistry of source waters and the degree of evaporative concentration. In some instances, and where brines are sourced by groundwater rather than seawater, the Mg/Ca of the dolomitising fluids is also influenced by interaction with non-carbonate basement rocks, as well as by the evaporative concentration (Logan, 1987; García

Del Cura *et al*., 2001). The chemical composition of seawater has changed through the Phanerozoic resulting in long-term fluctuation of the Mg/Ca ratio in phase with 100–200 My oscillations in sea-level, icehouse-greenhouse climates, and global volcanicity in relation to plate tectonics (Sandberg, 1983; Hardie, 1996). In addition to influencing the primary mineralogy of marine non-skeletal carbonates (aragonite, high-Mg calcite, low-Mg calcite), these fluctuations will also affect the dolomitisation potential of seawater-derived fluids (Steuber & Rauch, 2005). Some authors argue that, conversely, fluctuations in the mass of dolomite being formed influence the observed changes in seawater composition (Holland *et al.*, 1996; Holland & Zimmerman, 2000; Arvidson *et al*., 2011), with enhanced rates of dolomitisation during periods when climatic and tectonic conditions favoured brine generation (Sun, 1994).

In this paper, 1D numerical Reactive Transport Modelling (RTM) was used to explore the role of secular variations of seawater composition in controlling reflux diagenesis, including replacement dolomitisation and overdolomitisation, associated precipitation/dissolution of diagenetic sulphates, and implications for porosity modification. The dolomitising potential of brines formed during periods of aragonite and calcite seas was contrasted, based on evaporation of modern and Aptian seawaters (Mg/Ca of ~5 and ~1 respectively), and an intermediate fluid based on Mississippian seawater composition (Mg/Ca ~2). The sensitivity of the diagenetic system to salinity was explored, using brines ranging from mesosaline to hypersaline, generated by evaporative concentration of the three different Mg/Ca seawaters. This sensitivity to fluid composition is then contextualised by comparison with the impact of other extrinsic controls, such as temperature, pCO_2 and fluid flux rate. Finally the importance of intrinsic properties of the sedimentary system was explored, evaluating the effects of sediment texture on effective reactive surface area (RSA). Thus reflux diagenesis expected in

fine-grained, reactive but low permeability sediments, was compared with more coarse-grained sediments which may be less reactive but will likely experience higher fluid flux.

(A) METHODS

Reactive transport modelling (RTM) was performed using the numerical simulator TOUGHREACT (Xu *et al.*, 2004), which is capable of coupling chemical reactions and multiphase fluid flow, heat and solute transport in chemically and physically heterogeneous geologic domains. Temporal and spatial changes in porosity are calculated from changes in mineral volume fractions due to mineral precipitation and dissolution, considering feedbacks from evolving porosity and derived permeability.

The code has already been applied to simulate dolomitisation and associated diagenetic processes driven by geothermal convection, evaporative brine reflux and compactional flow in generic carbonate platforms (Wilson *et al.*, 2001; Jones & Xiao, 2005; Whitaker & Xiao, 2010; Al-Helal *et al.*, 2012a, b) and specific case studies (Consonni *et al.*, 2010). Here early shallow diagenesis driven by reflux of brines of different composition was simulated through sediments beneath the brine source, where the hydraulic drive has been demonstrated, by simulations of generic carbonate platforms, to be mostly vertical even for highly anisotropic systems ($k_{horizontal}/k_{vertical}$ 10^2-10^4; Al-Helal *et al.*, 2012b).

The model is a 1D vertical column, with an area of 1 m^2 and length of 10 m discretised into 1000 cells each 1 cm in length. An initial homogeneous 40% porosity was specified throughout the column. Flow rate is externally specified and constant through time: thus although permeability changes can be calculated from porosity they do not affect the simulation results.

All the simulations are isothermal, with the baseline having a temperature of 30 °C, and sensitivity to temperature was also investigated over the range of 20-40 °C. The model is

initially saturated with normal seawater (salinity of 35‰). In each simulation an evaporative brine of specified chemical composition was injected at the top of the column at a constant rate of 1 m/yr, with discharge at the bottom of the column. The flow rate is constrained by results of previous 2D simulations using comparable temperatures and salinities (Al-Helal *et al.*, 2012b), but sensitivity was explored over a range from 0.01 to 2 m/yr.

All simulations ran for 500 kyr using an automatic time stepping scheme dependent on the convergence behaviour of the chemical reaction system. For most of the simulations the specified initial mineralogy is 99% calcite and 1% "seed" dolomite, which provides nucleation sites, assuming prior stabilisation of primary high-Mg calcite and aragonite. The presence of small amounts of syndepositional dolomite is consistent with observations in modern dolomite-forming environments (Deffeyes *et al.*, 1965; Illing *et al.*, 1965; Shinn *et al.*, 1965; Carballo *et al.*, 1997; Mazzullo *et al.*, 1987). The formulation of equations for kinetic reactions in TOUGHREACT requires specification of a starting fraction of the mineral for calculating initial effective surface area. Preliminary simulations (not shown here) using less than 1% of dolomite "seed" show a longer induction period, i.e. at very early times dolomitisation proceeds less rapidly. Dolomitisation was also simulated in sediments which are entirely aragonitic or contain an equal fraction of calcite and aragonite. Gypsum and anhydrite were specified as secondary minerals that could precipitate when fluids become supersaturated, but which were not present at the beginning of the simulations.

Single cell batch simulations used a thermodynamic approach, whereby dolomite precipitation is solely controlled by the saturation state of the fluid and the fluid-rock system equilibrates within an individual model timestep. In the 1D simulations dolomite precipitation was modelled as a kinetic process, whereby dolomitisation rate is varied as a function of other model parameters. The kinetic rate constant for precipitation at 25 °C (4.58E-19 mol/m^2/s) and activation energy were extrapolated from the high-temperature (115-196 °C)

experiments of Arvidson & Mackenzie (1999), consistent with previous RTMs of dolomitisation (Jones & Xiao, 2005; Whitaker & Xiao, 2010; Al-Helal *et al.*, 2012a, b). The kinetic expression for dolomite precipitation is given by:

$$r_{\mathrm{dol}} = A_{\mathrm{s}} A e^{-\left(\frac{E_{\mathrm{a}}}{RT}\right)} \left(1 - \frac{Q}{K_{\mathrm{eq}}}\right)^{2.26} \qquad \text{(equation 1)}$$

where r_{dol} is the reaction rate of dolomite; A_{s} is the specific reactive surface area; Q is the activity quotient, and K_{eq} is the equilibrium constant for ordered dolomite; A, the pre-exponential factor, is 11.2 mol/cm^2/s; E_a, the activation energy, is 1.335 x 10^5 J/mol; R is the universal gas constant; T is the temperature (in Kelvin); and 2.26 is the reaction order (Arvidson & Mackenzie, 1999). Precipitation of dolomite was assumed to be the slowest diagenetic process modelled, and thus to limit the rate of calcite-aragonite dissolution, and gypsum-anhydrite precipitation where these reactions were thermodynamically favoured.

The code uses effective reactive surface area (RSA) to initialise nucleation of kinetic minerals. In the baseline simulation an effective RSA for dolomite of 500 cm^2/g, representative of small dolomite rhombs (50 μm diameter, based on geometric calculations) was specified. The sensitivity analysis tested the effect of varying dolomite RSA between a minimum of 100 cm^2/g and a maximum of 10,000 cm^2/g representing coarser (260 μm) and finer crystals (2.5 μm) respectively. RSA modifications due to diagenetic changes in texture are likely complex and are currently not incorporated in the simulations.

When simulating a mixture of primary calcite and aragonite, rate constants were specified also for these minerals. Calcite and aragonite dissolution kinetics have been subject to extensive experimental investigation and are better constrained than reaction kinetics of dolomite; however some uncertainty still remains even within well buffered systems (Arvidson *et al.*, 2003; Palandri & Kharaka, 2004). Moreover intrinsic rate variations in mineral dissolution are commonly up to 2.5 orders of magnitude (Lüttge *et al.*, 2013). Therefore, dissolution rates ranging between 1.0E-5 and 1.0E-11 mol/m^2/s have been tested

in this study. As for dolomite, RSA for calcite and aragonite was maintained equal to that of dolomite (500 cm^2/g), which is equivalent to spherical grains of 44 μm in diameter (precursor sediments are thus equivalent to coarse silts), needles of *ca.* 2 μm diameter, or larger but morphologically more complex grains.

Nine primary and 11 secondary aqueous species were incorporated in the geochemical calculations (Table 1). Thermodynamic data for the aqueous species and the 5 minerals (dolomite, calcite, aragonite, gypsum, anhydrite) were taken from the EQ3/6 geochemical database (Wolery, 1992) with some substitutions incorporated to account for recent published revisions in thermodynamic properties of rock-forming minerals and aqueous species. Details on data sources and the list of chemical species for which thermodynamic parameters have been updated are given in Xu *et al.* (2005). The simulations presented here use the Pitzer ion-interaction equation to calculate ionic activities, in contrast to most previous RTM studies (Wilson *et al.*, 2001; Whitaker & Xiao, 2010; Al-Helal *et al.*, 2012b), in which the Debye-Hückel approach employed underestimates the diagenetic potential of dolomitising fluids (Al-Helal *et al.*, 2012a).

Simulations were performed using three different source seawaters: modern, Mississippian and Aptian, with Mg/Ca molar ratios of 5.1, 2.3, and 1.2 respectively (Table 2). The major ion composition of modern seawater was derived from Nordstrom *et al.* (1979), while that of Aptian seawater was calculated from the chemical composition of fluid inclusions in Aptian marine halite (Timofeeff *et al.*, 2006). Mississippian seawater composition was taken from Demicco *et al.* (2005), who used an inverse model that considered variable cycling rates of seawater through axial portions of mid-ocean ridges. Seawater paleo-pH and atmospheric pCO_2 for the Mississippian and the Aptian (Table 2) were taken from Zeebe (2012), and they were used to calculate carbonate alkalinity using CO2SYS (Pierrot *et al.*, 2006) with dissociation constants from Mehrbach *et al.* (1973) refit by Dickson & Millero (1987). The

effects of changes in atmospheric pCO_2, leading to pH and carbonate alkalinity variations, were tested as part of the sensitivity analysis.

The composition of refluxing brines was derived by simulating evaporation of the three different seawaters (modern, Mississippian, and Aptian) by removal of pure water. This generated one mesosaline brine (44‰) and four hypersaline brines of 65, 89, 120 and 200‰. The 89‰ Mississippian brine was chosen as baseline for the sensitivity analysis of temperature, fluid flow rate, pCO_2, and effective RSA, because of its intermediate value of both Mg/Ca and salinity.

(A) RESULTS

(B) Seawater chemistry

All three source seawaters used in the simulations (modern, Mississippian and Aptian) at 30 °C are supersaturated with respect to calcite, aragonite and dolomite, and undersaturated with respect to gypsum and anhydrite. Compared with modern seawater, the degree of calcite supersaturation was slightly higher in the Aptian seawater, and slightly lower in the Mississippian seawater (Table 2). This reflects differences in absolute calcium concentration and pH determined by atmospheric pCO_2. However, the higher magnesium concentration of the modern seawater resulted in significantly greater dolomite supersaturation compared to both the Aptian and the Mississippian seawater.

Evaporative concentration of each of the three seawaters to salinities up to 200‰ leads to a progressive increase in the degree of saturation with respect with all the considered carbonate minerals (Fig. 1), enhancing differences in saturation state between the solutions. This suggests that for a given degree of evaporation, dolomitisation would be most rapid during periods when the seawater composition was similar to modern, and slowest when Mg/Ca ratio and pH were lower. The degree of undersaturation with respect to gypsum and anhydrite

decreases during evaporation, reaching gypsum equilibrium at salinities of 189‰, 159‰ and 188‰ for modern, Mississippian and Aptian seawaters respectively.

The diagenetic potential of these different fluids was first evaluated using closed system (batch) reactive transport simulations in which both calcite and dolomite were modelled as thermodynamic minerals. The total amount of dolomite that can be formed from 1 m^3 of normal modern seawater is 3.53E-03 m^3, while the same volume of Mississippian and Aptian normal seawaters would form 2.85E-03 and 2.66E-03 m^3 of dolomite respectively (Fig. 2). Differences in dolomitisation potential thus directly reflect contrasts in Mg/Ca between fluids, rather than saturation index. The evaporative concentration of each of these seawaters enhances the dolomitisation potential in direct proportion to the extent of evaporation, prior to any precipitation of gypsum (Fig. 2). The diagenetic potential of the same fluids during reflux was then evaluated using simple 1D reactive transport models.

Dolomitisation consumes Mg^{2+} and HCO_3^- and releases Ca^{2+} in all simulations, thus reducing the degree of dolomite supersaturation along the fluid flow path. As a result, dolomitisation rate decreases with distance beneath the brine source as long as overlying sediments remain only partially dolomitised. However, for most simulations, differences in reaction rate along the short (10 m) length of the modelled flow path are minor (see results for sensitivity to fluid flow below). For clarity, unless there is a significant depth dependence, changes in mineralogy (volume fraction of rock) and porosity (total volume %) are displayed for a single cell close to the base of the column (-9.5 m). At this depth the influence of any seasonal changes in boundary conditions (temperature, fluid composition), which may affect real sediments at shallow depth, can be ignored.

A 1 m/yr flux of modern seawater (Mg/Ca molar ratio of 5.1) at 30 °C resulted in complete replacement of precursor calcite within 111 kyr (Fig. 3B). This is accompanied by a porosity increase of up to 6% from an initial 40%, as expected from mineral density differences.

During replacement, a very minor amount of dolomite cement (<0.2 %) is also precipitated, limited by the relatively low Ca^{2+} concentration of the seawater. Following complete replacement, dolomite cementation accelerates, with precipitation of dolomite cement reducing porosity by 2.5% within 100 kyr of complete replacement. By the end of the simulation (at 500 kyr) the dolomite cement represents some 12% of the total dolomite volume, and has reduced the total porosity to 37% from a maximum of 46%. Dolomitisation rate increases exponentially during the period of replacement as the reaction progresses from about 0.4%/kyr with 25% dolomite to 1.25%/kyr and 1.8%/kyr at 50% and 75% dolomite respectively. This exponential increase reflects increasing total surface area with dolomite precipitation (equation 1). As dolomitisation rate increases, the Mg^{2+} concentration of fluid at the base of the simulated column decreases and the Ca^{2+} concentration increases.

Increasing brine concentration through evaporation of modern seawater enhances reaction rate independent of any increase in density-driven flux. The time to complete replacement of calcite by dolomite thus reduces with brine salinity (Figs 3 and 4A). Time is shown both in terms of absolute time and also time as a fraction of that required for complete replacement dolomitisation by normal modern seawater (1 in the top horizontal axis; Figs 3, 5, 7-10 and 12). For modern seawater, evaporation to 44‰ results in a complete calcite replacement by 86 kyr, while evaporation to 65‰ almost halves the time to complete replacement compared to normal seawater (Fig. 4A). Further concentration of source brines continues to accelerate replacement dolomitisation, although at a decreasing rate, so that for the most concentrated modern seawater simulated (200‰) all calcite is replaced within 24 kyr. The volume of dolomite cement precipitated also increases with increasing brine concentration, giving a net porosity reduction following complete replacement of calcite (Fig. 3D and E). The porosity loss 100 kyr after complete replacement shows a linear correlation with increasing brine salinity (Fig. 4B). Release of Ca^{2+} by replacement dolomitisation drives gypsum precipitation

from brines of 200‰ salinity, further occluding porosity (Fig. 3D and F). The gypsum reaches a maximum of 25% of the total rock volume by 24 kyr, but once calcite replacement is complete the reduction in Ca^{2+} driven by dolomite cementation leads to dissolution of the gypsum.

Reflux of brines formed by evaporation of Mississippian seawater (Mg/Ca molar ratio of 2.3) leads to synchronous precipitation of dolomite cement and replacement of calcite by dolomite (Fig. 5). During replacement there is initially a minor net porosity reduction and then porosity enhancement as replacement dolomitisation accelerates (50-0% calcite), followed by reduction in porosity by dolomite cementation. For Mississippian seawater complete replacement requires 463 kyr, although increasing brine concentration increases reaction rates and lowers the time to complete dolomitisation (Figs 4A and 5A). However, the rate of replacement is much slower than seen in the simulations of modern brines (Fig. 4A). Following complete replacement, the rate of porosity occlusion by dolomite cementation is also slower than that for modern brines (Fig. 4B). As with modern seawater, concentration of Mississippian seawater to 200‰ leads to gypsum precipitation during replacement dolomitisation (Fig. 5F). However, because of the higher calcium concentration of the 200‰ Mississippian brine, the mass of gypsum precipitated is sufficient to reduce porosity to 1% over the 110 kyr required for complete replacement dolomitisation (not shown, see Fig. S1 in the online supporting information). Further dolomitisation is limited by the rapid flow rate that results from this reduction in porosity.

Neither Aptian seawater (Mg/Ca molar ratio of 1.2) nor any of the brines generated from evaporation of Aptian seawater completely replace calcite within 500 kyr (Fig. 5, see also Fig. S2 in the online supporting information). Replacement dolomitisation is accompanied by calcite precipitation, which prohibits discrimination of replacement and cement dolomite volumes. The system is characterised by a net reduction in porosity ranging from 7 to 17%

for fluids of 35 to 120‰ at 500 kyr (Fig. 5D). For the 200‰ brine, this gradual reduction in porosity is augmented by precipitation of gypsum, which reaches almost 30% of the total rock volume and eliminates porosity by 500 kyr (Fig. 5F, see also Fig. S2 in the online supporting information).

(B) Sensitivity to initial carbonate mineralogy

Aragonite seas are characterized by abiotic carbonate precipitates of aragonite and high-Mg calcite. In contrast, calcite seas are characterized by abiotic precipitations of low-Mg calcite. Based on the Mg/Ca molar ratio, modern seawater is considered an aragonite sea, while the Aptian seawater is a calcite sea (Sandberg, 1983; Hardie, 1996). The Mississippian seawater, with Mg/Ca ~ 2, is at the threshold defined by Sandberg (1983) between a calcite and an aragonite sea. The influence of the precursor mineralogy on reflux dolomitisation was evaluated by simulations with an initial calcium carbonate composed entirely of aragonite, and mixed calcite-aragonite precursor allowing aragonite stabilisation to calcite as well as dolomitisation, for a range of brines (<200‰) derived from both modern and Mississippian seawaters.

In monomineralic systems, dolomite replaces aragonite faster than it replaces calcite irrespective of fluid composition (Fig. 6), reflecting a lower degree of supersaturation with respect to aragonite as compared to calcite (Fig. 1). Aragonite is replaced 2.4 ± 0.1 (mean ± 1 standard deviation) times quicker than calcite in simulations with modern fluids ranging from normal seawater (35‰) to 200‰ salinity (Fig. 6A), and 3.6 ± 0.1 times quicker than calcite in simulations with Mississippian brines from 35‰ to 120‰ salinity (excluding the Mississippian 200‰ brine; Fig. 6B). Following complete replacement of aragonite the rate of dolomite cementation is almost identical to that of calcite (results not shown).

To investigate the behaviour of a mixed $CaCO_3$ mineralogy system, Mississippian brine of 89‰ salinity was injected into the 1D model with an equal initial volume fraction of aragonite and calcite and 1% "seed" dolomite. Calcite and aragonite dissolution was modelled in this simulation as a kinetic process, and the sensitivity to different rate constants was also explored. Whilst sensitivity to different RSA for calcite and aragonite was not explicitly tested, increasing RSA of both minerals by one order of magnitude would give the same result as increasing both calcite and aragonite rate constants by one order of magnitude. Initially aragonite is replaced by calcite within 10 kyr for $CaCO_3$ rate constants ranging from 1.0E-5 to 1.0E-9 mol/m^2/s (Fig. 7). This is significantly faster than observations from the rock record would suggest (Walter & Burton, 1990). Once all the aragonite has been replaced, dolomite starts to replace calcite. Using lower rate constants than those obtained from laboratory experiments (e.g. 1.0E-10 mol/m^2/s), the aragonite remains in the system and is progressively replaced by both calcite and dolomite. All aragonite is lost within 54 kyr, after which calcite starts to be replaced by dolomite and replacement is complete by 228 kyr (Fig. 7). With the lowest used rate constant (1.0E-11 mol/m^2/s), calcite does not precipitate and dolomite replaces first aragonite and then calcite (Fig. 7).

(B) Sensitivity to temperature and pCO_2

The sensitivity of the shallow reflux system to temperature and pCO_2 was explored for the Mississippian brine of 89‰ salinity. Although over the simulated range from 20 to 40 °C both calcite and dolomite exhibit retrograde solubility, the strong temperature dependence of the rate of dolomitisation (equation 1) is reflected in a marked increase in the rate of both calcite replacement and dolomite cementation with temperature (Fig. 8). At 20 °C, complete replacement of calcite requires an estimated 537 kyr, and simultaneous dolomite cementation gives very slow porosity reduction. In contrast, at 40 °C complete replacement occurs within

55 kyr (three times the rate at 30 °C), and in the following 100 kyr, dolomite cement precipitation reduces porosity by some 11%.

Secular variations in atmospheric pCO_2 are reflected in differences in the pH and carbonate alkalinity of seawater (Foster, 2008; Zeebe, 2012), thus influencing carbonate diagenesis. Additionally, CO_2 production by bacteria and release from roots is known to elevate the pCO_2 of shallow pore waters by as much as 2 orders of magnitude compared with atmospheric values (Morse *et al.*, 1987). The Mississippian brine (89‰) was equilibrated with different pCO_2 values, from the present day atmospheric concentration of 350 to a maximum of 30,000 ppmv (reported in modern pore waters in shallow water sediments in the Bahamas and resulting from biogenic processes; Morse *et al.*, 1985). Despite reducing the dolomite saturation index (from +3.90 at atmospheric CO_2 to +2.48 at the highest pCO_2), there are only minor changes in the rate of dolomite replacement because the kinetic control dominates. In the simulation with 30,000 ppmv CO_2, complete replacement occurs within 154 kyr, only 11 kyr faster than the baseline (5,600 ppmv CO_2) and 27 kyr faster than the simulation with 350 ppmv CO_2 (Fig. 9). Equilibration with 30,000 ppmv CO_2, increases porosity from an initial value of 40% to 50% during calcite replacement, and then decreases by ~ 4% within the next 100 kyr due to dolomite cement precipitation (Fig. 9). In contrast, at low pCO_2 (350 and 1000 ppmv), prior to a period of rapid replacement, there is a systematic reduction of porosity due to precipitation of both dolomite and calcite (Fig. 9). After complete calcite replacement, porosity is further reduced by precipitation of dolomite cement down to 18% at 500 kyr at 350 ppmv CO_2, compared to 37% at 30,000 ppmv CO_2.

(B) Sensitivity to RSA and fluid flux

The extent to which the reactivity of the sediments influences the rate of dolomitisation during reflux was evaluated by varying the RSA. The baseline simulation was reflux of 89‰

Mississippian brine through sediments with an RSA of 500 cm^2/g, representative of dolomite rhombs of 50 μm diameter. In simulations employing lower RSA values, corresponding to coarser dolomite rhombs, the rate of replacement is slower (Fig. 10). Doubling the crystal size (halving the RSA) doubles the time to complete replacement. With an RSA of 100 cm^2/g (260 μm rhombs) only 18% dolomite is formed after 500 kyr. At such a low dolomitisation rate, calcite also precipitates, reducing porosity by 13% over 500 kyr. Following complete replacement of calcite, the rate of dolomite cementation also increases with RSA (Fig. 10D).

Fluid flux in natural systems will vary in a complex manner, not only with the gradient in effective head, but also the permeability of the sediments, which will evolve during diagenesis. To isolate this control, a time-invariant fluid flow rate was specified, with no feedback from changing rock properties during the simulation. Simulations suggest that at flow rates ≥0.5 m/yr the supply of Mg^{2+} does not limit reaction rates in the upper 10 m of sediment affected by reflux of 89‰ Mississippian brine (Fig. 11). In contrast, at lower flow rates the longer residence time of the fluids allows more rapid shallow dolomitisation, and thus rates in the lower part of the column are reduced due to Mg^{2+} depletion in fluids during shallower dolomitisation (Fig. 11). The rate of dolomite cementation and associated porosity loss scale directly with flow rate (Fig. 12). As a consequence, the sediment in the lower part of the column retains the porosity formed during replacement (8% for fluxes of ≤0.1 m/yr) even after 500 kyr of brine reflux (Fig. 12E). The absence of dolomite cementation with these low fluid fluxes is due to the consumption of most of the available Mg^{2+} in the first few centimetres of the flow path, where dolomite cement occludes almost completely the pore space.

(A) DISCUSSION

(B) Seawater chemistry

The main objective of this study was to evaluate how secular variations in seawater composition (specifically the changes in Mg/Ca molar ratio) may have affected dolomitisation and other associated diagenetic reactions in shallow reflux systems. Results from the 1D reactive transport modelling simulations show that Mg/Ca ratios >2.3 (modern and Mississippian seawaters) have the potential to replace calcite with dolomite and also precipitate dolomite cement within a few hundred thousand years. This timescale is consistent with results of previous RTM studies of reflux using modern brines (Jones & Xiao, 2005; Al-Helal *et al.*, 2012b). Replacement by brines generated from modern seawater (Mg/Ca = 5.1) is 4 ± 0.1 times more rapid than replacement by brines from Mississippian seawater (Mg/Ca = 2.3). Low Mg/Ca (1.2) Aptian seawater, despite being supersaturated in respect with dolomite, shows only limited dolomitisation potential. Rather, reflux of low Mg/Ca seawater and derived brines leads to precipitation of calcite, because the very low dolomitisation rate does not reduce the concentration of Ca^{2+} in the continuously supplied calcite supersaturated brines. Examples of Cretaceous calcite cements simultaneous to brine reflux dolomites are not known. Occurrence of synchronous dolomite and calcite cements has been reported instead in a few Cenozoic carbonates in meteoric-marine mixing zones, where dilution with meteoric water lowers Mg/Ca (Humphrey, 2000; Swart & Melim, 2000; Csoma *et al*., 2006). Dolomite and low-Mg calcite, in these cases, form at the same time following dissolution of the metastable aragonite and high-Mg calcite (Swart & Melim, 2000). Some models from this study, using a mixture of aragonite and calcite as precursor sediments and low reaction rates for these minerals, agree with these observations and show simultaneous replacement of aragonite by calcite and dolomite.

The models predict an increase in porosity during replacement of calcite by dolomite based on mineral density differences. However, the continued flux of dolomite supersaturated fluids after complete replacement causes precipitation of dolomite cement that occludes both

primary porosity and porosity generated by replacement dolomitisation. For Mississippian brines cementation by dolomite is simultaneous with replacement. This overdolomitisation has been reported proximal to paleo-brine pools in a number of studies of reflux dolomites (Lucia & Major, 1994; Saller & Henderson, 1998; Wahlman, 2010). Previous RTM studies also predicted the precipitation of dolomite cements proximal to the brine source, although this required either high fluid flux, high temperatures or long (several million years) time periods (Jones & Xiao, 2005; Al-Helal *et al.*, 2012b).

A constant fluid flux was specified in the simple models of this study, and the outcome of a diagenetic increase in porosity is thus longer fluid residence times. In these simulations, this effect will enhance rates of replacement of calcite by dolomite, and the rate of dolomite cementation may also be increased by the longer residence times of diagenetic fluids. At these relatively low temperatures the rate of replacement dolomitisation is limited by kinetics rather than Mg^{2+} flux, as seen by the relatively low sensitivity to flux (Fig. 12). The simulations of replacement dolomitisation are thus unlikely to be significantly affected by ignoring the feedback between porosity, permeability and flux. However, at low porosity the 1D models of this study may underestimate the rate of dolomite cementation at very shallow depth beneath the brine pool and overestimate it at greater depth.

In natural systems diagenetic alteration of permeability would likely alter the distribution of fluid flux, enhancing reaction rates in more permeable areas and limiting those in less permeable regions. The significance of these effects is demonstrated by 2D simulations of Jones & Xiao (2005) which specify a random initial permeability distribution and show the formation of pronounced perturbations in the geometry of the dolomite front (dolomite fingers) for an externally specified brine injection rate. More recent 2D simulations of sediments with depositional textural variations show that permeability alteration changes total fluid flux in response to a specified density gradient, in addition to redistributing diagenetic

alteration (Gabellone *et al.*, 2014b). The evolution of permeability resulting from dolomitisation appears to be strongly dependent on both depositional and diagenetic texture, and these controls are currently not fully understood (Woody *et al*., 1996; Gregg, 2004). There is the need to focus future research on textural changes resulting from dolomitisation and consequent permeability modification.

For each of the three seawaters examined, evaporative concentration enhances dolomite supersaturation and thus the rate of replacement dolomitisation, independent of the effect of enhanced density-driven fluid flux. This result agrees with previous models of brine reflux dolomitisation using modern brines with different salinity in a generic 2D carbonate platform (Jones & Xiao, 2005). The 1D simulations suggest that for both modern and Mississippian seawaters the time to replace all calcite is inversely proportional to salinity, where the exponent of the power law is higher for the more Mg-rich modern waters (Fig. 4A). The rate of dolomite cementation also increases with brine salinity. However, evaporative concentration of brines derived from Mississippian seawater beyond 159‰ results in supersaturation with respect to gypsum; gypsum precipitation rapidly occludes porosity and inhibits further dolomitisation. Previous RTM studies of modern brine reflux show porosity occlusion by precipitation of anhydrite downstream of the zone of dolomitisation, and progressive anhydrite dissolution and reprecipitation ahead of the advancing dolomite front due to continued reflux (Jones & Xiao, 2005; Al-Helal *et al*., 2012b). Diagenetic evaporites in association with brine reflux dolomites have been reported in several case studies (Leary & Vogt, 1987; Cantrell *et al*. 2004; Ehrenberg, 2006; Ehrenberg *et al*., 2006; Rahimpour-Bonab *et al*. 2010). These have been explained by the release of calcium during dolomitisation which reacts with the available sulphate in the brines to precipitate gypsum and anhydrite (Machel, 1986; Leary & Vogt, 1987). Anhydrite, which is usually formed by stabilisation of gypsum, commonly occurs as pore-filling cement in nodules or patches, and can negatively

impact reservoir quality (Ehrenberg, 2006). The spatial distribution of evaporite cements (evenly or patchy) critically affect porosity-permeability relationships. More evenly distributed anhydrite cements will tend to reduce pore-throat size, porosity, and permeability, whilst patchy anhydrite distribution will reduce porosity without significantly altering pore-throat size and reducing permeability only slightly (Lucia, 1999).

The rate of simulated replacive dolomite formation from any given fluid (below gypsum saturation) increases exponentially driven by the increasing dolomite abundance:

$$Dol_t = Dol_0 \, e^{(xt)} \qquad \text{(equation 2)}$$

where Dol_t is the dolomite volume fraction at time t, Dol_0 is the initial ("seed") dolomite volume fraction, and time t is in kyr. For any given source seawater, the value of the exponent x is determined directly by the degree of evaporative concentration (represented by the salinity of the brine in Fig. 13A). Differences between Mg/Ca of the source seawater define the relationship between the gradient a of the relationship between exponent x and brine salinity (Fig. 13B).

Based on the exponential form of this relationship (equation 2), beds where dolomitisation occurs at a higher initial rate would be anticipated to continue to dolomitise with increasingly rapidity, reflecting the increasing dolomite total reactive surface area (equation 1). This positive feedback would favour the development of stacked sequences in which limestone beds that have been completely replaced alternate with those where dolomite abundance remains low, rather than the development of thick partially dolomitised sequences. This prediction accords with the fossil record where reports of partial dolomitisation generally refer to alternation of beds that are largely or completely dolomitised with beds where dolomite is rare or sparse, rather than extensive sequences that are partially dolomitised (Montañez & Read, 1992; Garcia-Fresca *et al*., 2009; Saller & Dickson, 2011; Iannace *et al*., 2014; Haas *et al*., 2015). The exponent x in equation 2 is controlled by both Mg/Ca and

salinity, suggesting that the propensity for interbedded limestones and dolomite will be greater for where diagenetic fluids are high salinity brines, especially where these brines formed from seawaters with high Mg/Ca. However, the simple models of this study do not consider the dynamic nature of shallow water carbonate sedimentation, in which eustatic sea level fluctuations control both sediment accumulation and synsedimentary diagenesis. Thus, sequences of alternating dolomitised and undolomitised beds could also reflect alternation of platform-top brine composition during progradation-retrogradation cycles (Montañez & Read, 1992; Rameil, 2008). Coupling of sedimentary models and RTMs allowes a more accurate evaluation of the evolution of reflux dolomitisation in a sequence stratigraphic context, by employing temporally evolving platform geometry and boundary conditions (Palmer *et al*., 2014; Frazer *et al*., 2015).

Results from this study suggest that, based only on the geochemical composition of seawater, larger volumes of dolomite would be expected in reflux systems developed at times of aragonite seas (high Mg/Ca) than in comparable systems during periods of calcite seas (low Mg/Ca). High temperature laboratory experiments have indeed shown increased rate of dolomitisation with increasing Mg/Ca of the solution (Gaines, 1980; Sibley *et al.*, 1994; Lumsden *et al*., 1995; Kaczmarek & Sibley, 2011).

Equation 2 was combined with the secular variations in seawater Mg/Ca from Hardie (1996; Fig. 14A) to calculate the changes through time of the abundance of replacive dolomite that would form over 100 kyr. These changes are illustrated for normal marine seawater (35‰) and two evaporative brines (89 and 120‰), assuming 1% dolomite "seed" and 40% initial porosity (Fig. 14B). The resulting predicted changes in potential dolomite abundance clearly reflect the secular changes in Mg/Ca, but the rate of change in predicted dolomitisation rate over time is enhanced compared to the Mg/Ca changes because of the non-linear relationship between dolomitisation rate and Mg/Ca. This effect is even more marked for the high salinity

brines than for normal seawater, suggesting that for high salinity brines formed during periods of high Mg/Ca the rates of dolomitisation would be very fast (complete calcite replacement in less than 100 kyr). However, the comparison of the calculated dolomite rates (Fig. 14B) with the observed dolomite abundance in the geologic record (Given & Wilkinson, 1987; Fig. 14C) clearly shows a lack of correlation, suggesting that controls other than the geochemical potential of the fluids exert a stronger effect on secular variations in dolomitisation.

The geologic record does contain numerous examples of reflux dolomites formed during calcite seas, for instance the Early-Middle Cretaceous (Fisher & Rodda, 1969; Sun, 1995; Rameil, 2008; Vandeginste *et al*., 2013; Iannace *et al*., 2014). Reflux dolomites have been documented as well in the Mississippian (Sun, 1995; Sonnenfeld, 1996; Al-Aasm & Packard, 2008; Rott & Qing, 2013), which is a period when chemistry was shifting from calcite to aragonite sea. The geologic record also contains examples of extensive carbonate deposits formed in aragonite seas that do not contain large amounts of dolomite. Compared to the rest of the Phanerozoic, the Cenozoic is a period of time with lesser amounts of dolomite (Given & Wilkinson, 1987). Large volumes of dolomite in modern reflux settings (aragonite sea) are also rare (Kocurko, 1979; Lucia & Major, 1994; Rivers *et al.*, 2012). These apparent paradoxes arise because there are multiple controls on dolomitisation in addition to fluid chemistry. Some of these other parameters, most importantly eustatic sea-level and temperature, also show secular variations. However, their effects on dolomitisation are inversely related to those of the associated change in seawater chemistry. Greenhouse periods such as the Early Cretaceous are characterised by not only calcite seas (low Mg/Ca), but also higher global temperature which is kinetically favourable for dolomitisation. The high sea-level resulting from thermal expansion, in association with low amplitude eustatic variations, would also favour the development of extensive shallow-water carbonate platforms and

sustained brine reflux. Recent studies of magnesium isotopes in the Cenozoic (Pogge von Strandmann *et al*., 2014) link the rapid decline in dolomitisation in the early-mid Oligocene and present day to global cooling. Finally, the relationship between periods of reduced atmospheric/ocean oxygen levels and increased dolomite abundance was suggested by Burns *et al.* (2000) to reflect abundance of microbial sulphate reduction, with increased nucleation sites for dolomite formation as a result of microbial dolomitisation. These kinetic controls may be key parameters given the relatively slow initiation period for dolomitisation (Sibley *et al.*, 1987; Kaczmarek & Sibley, 2011).

Similarly, the lack of dolomitisation in the recent may be associated with icehouse sea-level fluctuations. Although modern refluxing brines show magnesium depletion indicative of dolomitisation (e.g. Whitaker *et al*., 2014), the rapidity of recent sea-level rise has given insufficient time to substantially dolomitise carbonates within and underlying modern brine lagoons (Warren, 2000). Low amplitude eustatic fluctuations in sea-level serve not only to extend the duration of emersion of carbonate sediments in seawater/brines, but might also preserve them from dissolution and/or dedolomitisation by meteoric fluids which are characteristically dolomite undersaturated (Hardie, 1987; Deike, 1990).

During icehouse periods lower atmospheric pCO_2 causes an increase of the saturation state of seawater with respect to all carbonate minerals (Given & Wilkinson, 1987) and it has been suggested that these conditions may favour synsedimentary dolomite formation (Mackenzie & Pigott, 1981; Machel & Mountjoy, 1986). Numerical simulations comparing the effect of aragonite and calcite as precursor minerals for reflux dolomitisation suggest that although aragonite is dolomitised faster than calcite, aragonite tends to be replaced by calcite at rates significantly faster than those of dolomitisation. Once aragonite has been completely lost dolomitisation continues by replacement of calcite, confirming that precursor mineralogy is likely not an important control on replacement dolomitisation. Indeed it is now recognised

that aragonite supersaturation in the modern ocean results not from low pCO_2 but from high Mg/Ca which inhibits calcite precipitation (Morse *et al.*, 1997). In turn, there is increasing evidence (e.g. Holland, 2005; Pogge von Strandmann *et al*., 2014) to support the suggestion of Wilkinson & Algeo (1989) that dolomitisation is a driver, rather than a consequence, of major secular changes in seawater Mg/Ca.

(B) Sensitivity analysis

Shallow reflux dolomitisation systems are sensitive to changes in seawater chemistry, but this control operates within the context of other extrinsic and intrinsic controls. In contrast to natural systems, numerical simulations provide the opportunity to evaluate the relative importance of individual parameters. Results from a sensitivity analysis using 89‰ Mississippian brine as the baseline are summarised in tornado charts (Fig. 15). The time required to replace all calcite for the baseline simulation (165 kyr) is represented by the black vertical line, and horizontal bars show the range of replacement times spanned by simulations over the specified range of parameter values.

Rates of replacement of sediments with an effective RSA from 10,000 cm^2/g to 250 cm^2/g, corresponding to dolomite rhombs from 2.5 μm to 100 μm respectively, significantly affect the time to reach complete replacement of calcite by dolomite. Over the range of parameter values investigated, the RSA is almost as important as the degree of evaporative concentration of brine (salinity from 35‰ to 120‰). The importance of this control has also been demonstrated in 2D simulations, where higher initial RSA results in greater lateral extension of dolomite bodies from the brine source at specific time slices (Jones & Xiao, 2005; Al-Helal *et al*., 2012b). Fine-grained sediments are more reactive and tend to be dolomitised at a faster rate than coarse-grained sediments according to a power law (Fig. 10F). This accords with many observations of preferential dolomitisation of mudstone beds in

the rock record (e.g. Hopkins, 2004; Cantrell *et al*. 2004; Smith *et al.*, 2004). In contrast, dolomitised grainstone beds within more muddy limestones (e.g. Sharp *et al*., 2010; Hollis *et al*., 2011; Martín-Martín *et al.*, 2013) are less common and tend to be associated with higher temperature systems where alteration is likely flux rather than reaction rate limited. However, simple assumptions relating reactivity to grain size can be misleading. Thus for example the RSA of an ooid grainstone derived geometrically from the grain diameter might be a significant underestimate where algal boring of the outer cortex provides dolomitising fluids access to the complex inner structure of the ooid (Griffiths *et al.*, 2013). In natural systems, RSA will also change during dolomitisation, with a progressive increase in rhomb size serving to reduce the rate of dolomitisation, at a stage when simulations predict it to be most rapid. Incorporation of these complexities in future models offers an opportunity to evaluate such feedbacks, particularly if coupled with laboratory experiments.

Although simulations evaluate a relatively limited temperature range (20-40 °C), the effect on dolomitisation rate is comparable to that of a forty times change in RSA (from 250 to 10,000 cm^2/g), with higher temperatures speeding up dolomitisation according to a power relationship (Fig. 8F). Previous simulations of brine reflux in a generic 2D platform showed a direct dependence of dolomitisation rate on platform top-temperature above a threshold of *ca.* 30 °C, although at 45 °C the dolomitisation rate declines due to anhydrite precipitation (Al-Helal *et al*., 2012b). Variations in sea-surface temperature over geologic time can be inferred from paleoclimatic reconstruction, so that times more favourable for dolomitisation can be hypothesised. In addition to a temporal and latitudinal control on climate, seasonal variations can be significant. Annual temperature variation in modern sabkhas of the Arabian Gulf can be extreme, with summer surface temperatures often exceeding 50 °C but falling below 10 °C at night during the winter (Lokier, 2012). The paleoclimatic regime is critical in determining whether temperature and brine concentration maxima are coincident at times of maximum

solar insolation, or whether seasonal rainfall at these times would dilute platform top fluids and reduce geochemical potential for reflux dolomitisation.

Within the simulated 10 m depth, dolomitisation rate appears to be controlled by fluid flow only at very low fluxes (≤0.01m/yr; Fig. 12). This is in agreement with the simulations performed by Jones & Xiao (2005), that show a substantial decrease in the rate of dolomite formation (-0.65 volume %/kyr) when specifying initial flow velocities on the order of centimetres-per-year rather than meters-per-years. This result, particularly when coupled with the lower RSA for many grainstones, challenges the explanation of cases where brine reflux has preferentially dolomitised more permeable grainstone units. Such instances may indicate that the dolomitising system is flux limited, perhaps due to a low head gradient that may characterise extensive brine pools lacking a physical barrier to circulation, and indicate that dolomitisation rates may be slow (Gabellone *et al.*, 2014b). However, at a higher flow rate the shallow reactions consume less Mg^{2+}, allowing replacement dolomitisation to extend to greater depth below the simulated section.

Simulations suggest that variation of pH and carbonate alkalinity associated with changes in pCO_2 has little impact on the rate of replacement dolomitisation in the shallow subsurface (Fig. 9). However biologically-mediated formation of dolomite or very-high-Mg calcite, which may be critical in generating dolomite "seeds" (Vasconcelos & McKenzie, 1997; Bontognali *et al.*, 2012) or even in contributing to massive dolomitisation in sediments beneath lagoons (McKenzie & Vasconcelos, 2009), is beyond the scope of the current model.

Over the range of values explored in this suite of simulations, the rate of post-replacement dolomite cementation shows lower sensitivity to changes in controlling parameters than does the rate of replacement (Fig. 15B). The exception is fluid flux, which provides a direct control on cementation rate, with higher fluxes yielding higher rates of post-replacement cementation. This appears to favour cementation in areas of high head gradient and in

sediments with an initial high permeability. Thus, as long as replacement dolomitisation is not flux limited, it will favour more reactive sediments that may also have initially been less permeable, whilst cementation may preferentially affect more permeable units. The effect of reflux on dolomitisation will thus vary spatially from areas immediately underlying the brine pool where brines will be forced vertically through beds which may have differing reactivity irrespective of their permeability, to areas downstream of the brine pool where lateral (bedding parallel) flow will be focussed along more permeable units (Gabellone *et al*., 2014b). At times of favourable brine composition, this flux dependence is likely to result in precipitation of dolomite cement in the more permeable grainstones, but at a much slower rate in the low permeability mudstones due to low fluid fluxes. During subsequent episodes of replacement, the previously formed dolomite cements serve as *nuclei* and favour preferential dolomitisation of the grainstones.

In natural systems there will be links between some of the parameters which here have been evaluated independently. One example is the likely, though not inevitable, inverse correlation between RSA and permeability resulting from a common grain size control. Fine-grained sediments are highly reactive providing potential for more rapid replacement dolomitisation than coarse-grained sediments. However, this effect may be offset by the lower permeability of finer sediments which will limit rates of fluid flow for a given effective head gradient. Contrastingly, fluid flux and brine salinity are positively correlated, as evaporative concentration provides the density gradient to drive flow as well as increasing both absolute concentrations of reactive solutes and the Mg/Ca. This effect will directly increase dolomite cementation, but only affect replacement dolomitisation in systems where this reaction is flux limited. Similarly, increased solar insolation will result in both kinetically favourable high temperatures and higher rates of evaporation which will favour formation of more saline

brines. These synergies should be considered when applying results of these numerical experiments investigating individual controls to natural systems.

The veracity of RTM predictions of absolute rates of dolomitisation remains limited by the still poor understanding of thermodynamics and especially kinetics of the process at the relatively low temperatures of systems modelled here. Consonni *et al.* (2010) show how variations of the precipitation and dissolution kinetic constants of dolomite by five orders of magnitude considerably affects the rate and dynamics of the dolomitisation process, with faster kinetics giving sharp dolomitisation fronts in contrast to large zones of partial dolomitisation resulting from slower kinetics. Here the use of kinetic rates from Arvidson & Mackenzie (1999) allows a direct comparison with previous RTM studies of dolomitisation (Wilson *et al.*, 2001; Jones & Xiao, 2005; Whitaker & Xiao, 2010, Al-Helal *et al.*, 2012a, b). The annotation of the time axis in terms of time to complete replacement of calcite by dolomite relative to that required by normal modern seawater in the graphs showing the predicted changes in mineralogy through time (Figs 3, 5, 7-10, 12) should facilitate future comparisons as understanding of thermodynamics and kinetics of dolomitisation evolves.

(A) CONCLUSIONS

One-dimensional reactive transport modelling of vertical brine reflux in shallow carbonate systems allowed evaluation of the control of secular variations in seawater chemistry on dolomitisation and associated porosity modification. Simulations suggest faster replacement of calcite by dolomite during periods of aragonite seas than in periods of calcite seas, solely in response to changes in seawater Mg/Ca. In all the modelled scenarios, replacement dolomitisation is accompanied by increase in porosity, which is then reduced by precipitation of dolomite cement. The rates of both replacement and dolomite cementation are enhanced by increasing brine salinity, irrespective of associated higher rates of density-driven fluid flow.

Other factors exerting a major control on dolomitisation rates in shallow reflux systems include effective reactive surface area of precursor sediments and temperature. The control of fluid flux seems to be significant only at very low flux rates, whilst changes of pH and carbonate alkalinity associated with variation in pCO_2 appear to have only a minor impact. Higher Mg/Ca in aragonitic seas would appear to favour dolomitisation from seawater-derived fluids. However, the impact of other controls such as temperature and the eustatic sea-level support evidence for formation of significant volumes of dolomite during periods of calcitic seas. Simulations thus support the hypothesis originally advanced by Wilkinson & Algeo (1989) that dolomitisation is a driver rather than a consequence of major secular changes in seawater Mg/Ca.

An important limitation of these simulations relates to parameterisation of the kinetic rate law which derived from experiments at significantly higher temperatures than the modelled system (Arvidson & Mackenzie, 1999). This introduces uncertainty in absolute rates of dolomitisation, although the general form of the relationships is likely more robust. Furthermore the effects of biological mediation, which have been suggested to be important in some studies of recent dolomitisation (e.g. Vasconcelos & McKenzie, 1997; Bontognali *et al.*, 2012) are not considered. Notwithstanding, the simple numerical experiments presented can provide an important contribution to unravelling diagenesis, enabling the evaluation of individual parameters and the generation of a physically and chemically-based set of guiding principles. Numerical models in general also serve to highlight those parameters which are likely to be of particular importance and direct future work. For example, this study suggests that effective RSA is a critical control on dolomitisation, suggesting the importance of depositional textures in reaction-rate limited system. However, our understanding of reactivity is yet poorly developed. This systematic evaluation has laid the foundation for future simulations to explore the effect of interactions between individual controls. In this

respect, simulations of specific case studies can provide constraints on realistic spatial facies distribution, allowing exploration of how depositional textures affect the pattern of dolomitisation through the combined control of both fluid flux *via* permeability architecture and reaction rate *via* the effective surface area.

ACKNOWLEGEMENTS

We thank BG Group, Chevron, Petrobras, Saudi Aramco and Wintershall for sponsorship of the University of Bristol ITF (Industry Technology Facilitator) project IRT-MODE. The Editor Tracy Frank, Associate Editor Giovanna Della Porta, David Budd and two anonymous reviewers are acknowledged for their constructive reviews.

List of Symbols

r_{dol}	reaction rate of dolomite
A_{s}	specific reactive surface area
Q	activity quotient
K_{eq}	equilibrium constant
A	pre-exponential factor
E_a	activation energy
R	universal gas constant
T	temperature (Kelvin)
Dol_t	dolomite volume fraction at time t
Dol_0	initial dolomite volume fraction
t	time (kyr)

REFERENCES

Adams, J.E. and **Rhodes, M.L.** (1960) Dolomitization by seepage reflux. *AAPG Bull.*, **44**, 1912-1920.

Al-Aasm, I.S. and **Packard, J.J.** (2008) Reflux dolomitization of Mississippian-age sabkha and restricted subtidal sediments resulting in a 1.6 TCF giant gas field: Geologic and geochemical evidence from the Upper Debolt Formation of West-Central Alberta, Canada. *GeoArabia, First and Second International Conference on Evaporites, 2004 and 2006, United Arab Emirates, Abstract*, **13**, 143.

Al-Helal, A.B., Whitaker, F.F., Spycher, N. and **Xiao, Y.** (2012a) Modeling brine reflux using the Pitzer Ion-Interaction model in TOUGHREACT. In: *Proceedings of the TOUGH Symposium 2012*, (Eds S. Finsterle, D. Hawkes, G. Moridis, S. Mukhopadhyay, C. Oldenburg, L. Peiffer, J. Rutqvist, E. Sonnenthal, N. Spycher, C. Valladao and L. Zheng), pp. 841-847, Lawrence Berkeley National Laboratory, Berkeley, California, 17-19 September.

Al-Helal, A.B., Whitaker, F.F. and **Xiao, Y.** (2012b) Reactive transport modeling of brine reflux: Dolomitization, anhydrite precipitation, and porosity evolution. *J. Sed. Res.*, **82**, 196-215.

Amthor, J.E., Mountjoy, E.W. and **Machel, H.G.** (1994) Regional-scale porosity and permeability variations in Upper Devonian Leduc buildups: Implications for reservoir development and prediction in carbonates. *AAPG Bull.*, **78**, 1541-1558.

Arvidson, R.S. and **Mackenzie, F.T.** (1999) The dolomite problem: Control of precipitation kinetics by temperature and saturation state. *Am. J. Sci.*, **299**, 257-288.

Arvidson, R.S., Ertan, I.E., Amonette, J.E. and **Lüttge, A.** (2003) Variation in calcite dissolution rates: A fundamental problem? *Geochim. Cosmochim. Acta*, **67**, 1623-1634.

Arvidson, R.S., Guidry, M.W. and **Mackenzie, F.T.** (2011) Dolomite controls on Phanerozoic seawater chemistry. *Aquat. Geochem.*, **17**, 735-747.

Bontognali, T.R.R., Vasconcelos, C., Warthmann, R.J., Lundberg, R. and **McKenzie, J.A.** (2012) Dolomite-mediating bacterium isolated from the sabkha of Abu Dhabi (UAE). *Terra Nova*, **24**, 248-254.

Burns, S.J., McKenzie, J.A. and **Vasconcelos, C.** (2000) Dolomite formation and biogeochemical cycles in the Phanerozoic. *Sedimentology*, **47**, 49-61.

Cantrell, D., Swart, P. and **Hagerty, R.** (2004) Genesis and characterization of dolomite, Arab-D Reservoir, Ghawar field, Saudi Arabia. *GeoArabia*, **9**, 11-36.

Carballo, J.D., Land, L.S. and **Miser, D.E.** (1987) Holocene dolomitization of supratidal sediments by active tidal pumping, Sugarloaf Key, Florida. *J. Sed. Petrol.*, **57**, 153-165.

Consonni, A., Ronchi, P., Geloni, C., Battistelli, A., Grigo, D., Biagi, S., Gherardi, F. and **Gianelli, G.** (2010) Application of numerical modelling to a case of compaction-driven dolomitization: a Jurassic palaeohigh in the Po Plain, Italy. *Sedimentology*, **57**, 209-231.

Csoma, A.E., Goldstein, R.H. and **Pomar, L.** (2006) Pleistocene speleothems of Mallorca: implications for palaeoclimate and carbonate diagenesis in mixing zones. *Sedimentology*, **53**, 213-236.

Dawans, J.M. and **Swart, P.K.** (1988) Textural and geochemical alternations in Late Cenozoic Bahamian dolomites. *Sedimentology*, **35**, 385-403.

Deffeyes, K.S., Lucia, F.J. and **Weyl, P.K.** (1965) Dolomitization of Recent and Plio-Pleistocene sediments in marine evaporite waters on Bonaire, Netherlands Antilles. In: *Dolomitization and limestone diagenesis* (Eds L.C. Pray and R.C. Murray), *SEPM Spec. Publ.*, 13, 71-88.

Deike, R.G. (1990) Dolomite dissolution rates and possible Holocene dedolomitization of water-bearing units in the Edwards aquifer, south-central Texas. *J. Hydrol.*, **112**, 335-373.

Demicco, R.V., Lowenstein, T.K., Hardie, L.A. and **Spencer, R.J.** (2005) Model of seawater composition for the Phanerozoic. *Geology*, **33**, 877-880.

Dickson, A.G. and **Millero, F.J.** (1987) A comparison of the equilibrium constants for the dissociation of carbonic acid in seawater media. *Deep-Sea Research Part a-Oceanographic Research Papers*, **34**, 1733-1743.

Ehrenberg, S.N. (2006) Porosity destruction in carbonate platforms. *J. Petrol. Geol.*, **29**, 41-52.

Ehrenberg, S.N., Eberli, G.P., Keramati, M. and **Moallemi, S.A.** (2006) Porosity-permeability relationships in interlayered limestone-dolostone reservoirs. *AAPG Bull.*, **90**, 91-114.

Fisher, W.L. and **Rodda, P.U.** (1969) Edwards Formation (Lower Cretaceous), Texas. Dolomitization in a Carbonate Platform System. *AAPG Bull.*, **53**, 55-72.

Foster, G.L. (2008) Seawater pH, pCO_2 and CO_3^{2-} variations in the Caribbean Sea over the last 130 kyr: A boron isotope and B/Ca study of planktic forminifera. *Earth Planet. Sci. Lett.*, **271**, 254-266.

Frazer, M.A., Whitaker, F.F. and **Hollis, C.** (2015) Development of syn-depositional models of carbonate diagenesis: An application of PyTOUGH to complex geological processes. In: *TOUGH Symposium*. Lawrence Berkeley National Laboratory, Berkeley, California, 28-30 September.

Gabellone, T., Iannace, A. and **Gasparrini, M.** (2014a) Multiple dolomitization episodes in deep-water limestones of the Triassic Lagonegro basin (southern Italy): From early reflux to tectonically driven fluid flow. *J. Sed. Res.*, **84**, 435-456.

Gabellone, T., Griffiths, G., Whitaker, F., Katz, D.A. and **Sonnenfeld, M.** (2014b) Controls on the distribution of reflux dolomitisation: Insights from modelling the marvellous Madison. In: *AAPG Annual Conference and Exhibition, Search and Discovery Article #90189*, Houston, Texas, 6-9 April.

Gaines, A.M. (1980) Dolomitization kinetics: recent experimental studies. In: *Concepts and models of dolomitization,* (Eds D.H. Zenger, J.B. Dunham and R.L. Ethington), *SEPM Spec. Publ.*, 28, 81-86.

García Del Cura, M.A., Calvo, J.P., Ordóñez, S., Jones, B.F. and **Cañaveras, J.C.** (2001) Petrographic and geochemical evidence for the formation of primary, bacterially induced lacustrine dolomite: La Roda 'white earth' (Pliocene, central Spain). *Sedimentology*, **48**, 897-915.

Garcia-Fresca, B., Jones, G.D. and **Tianfu, X.** (2009) The apparent stratigraphic concordance of reflux dolomite: New insights from synsedimentary reactive transport models. In: *AAPG Convention, Search and Discovery Article #50208,* Denver, Colorado, 7-10 June.

Given, R.K. and **Wilkinson, B.H.** (1987) Dolomite abundance and stratigraphic age: constraints on rates and mechanisms of Paleozoic dolostone formation. *J. Sed. Petrol.*, **57**, 1068-1078.

Gregg, J.M. (2004) Basin fluid flow, base-metal sulphide mineralization and the development of dolomite petroleum reservoirs. In: *The geometry and petrogenesis of dolomite hydrocarbon reservoirs* (Eds C.J.R. Braithwaite, G. Rizzi, and G. Darke), *Geol. Soc. London Spec. Publ.*, 235,157-175.

Griffiths, G., Whitaker, F., Gabellone, T., Katz, D. and **Sonnenfeld, M.** (2013) Intrinsic and extrinsic controls on the regional scale distribution of reflux dolomitisation: Insights from modelling the marvellous Madison. In: *Conference abstract volume of the 30th IAS Meeting of Sedimentology,* Manchester, 2-5 September.

Haas, J., Lukoczki, G., Budai, T. and **Demény, A.** (2015) Genesis of Upper Triassic peritidal dolomites in the Transdanubian Range, Hungary. *Facies*, **61**, 1-28.

Halley, R.B. and **Schmoker, J.W.** (1983) High-porosity Cenozoic carbonate rocks of South Florida: progressive loss of porosity with depth. *AAPG Bull.*, **67**, 191-200.

Hardie, L.A. (1987) Dolomitization: A critical view of some current views. *J. Sed. Petrol.*, **57**, 166-183.

Hardie, L.A. (1996) Secular variation in seawater chemistry: An explanation for the coupled secular variation in the mineralogies of marine limestones and potash evaporites over the past 600 My. *Geology*, **24**, 279-283.

Holland, H.D. (2005) Sea level, sediments and the composition of seawater. *Am. J. Sci.*, **305**, 220-239.

Holland, H.D. and **Zimmerman, H.** (2000) The dolomite problem revisited. *Int. Geol. Rev.* **42**, 481-490.

Holland, H.D., Horita, J. and **Seyfried, W.E.** (1996) On the secular variations in the composition of Phanerozoic marine potash evaporites. *Geology*, **24**, 993-996.

Hollis, C., Frazer, M., Gawthorpe, R., Al-Hajri, A., Hodgetts, D., Hirani, J., Juerges, A. and **Newport, R.** (2011) The relationship between structural evolution and diagenesis: some thoughts with respect to the Arabian Plate. In: *North Africa Fracture Workshop*, Manchester, 12-13 January.

Hopkins, J.C. (2004) Geometry and origin of dolomudstone reservoirs: Pekisko Formation (Lower Carboniferous), western Canada. In: *The geometry and petrogenesis of dolomite hydrocarbon reservoirs* (Eds C.J.R. Braithwaite, G. Rizzi, and G. Darke), *Geol. Soc. London Spec. Publ.*, 235, 349-366.

Humphrey, J.D. (2000) New geochemical support for mixing-zone dolomitization at Golden Grove, Barbados. *J. Sed. Res.*, **70**, 1160-1170.

Iannace, A., Frijia, G., Galluccio, L. and **Parente, M.** (2014) Facies and early dolomitization in Upper Albian shallow-water carbonates of the southern Apennines (Italy): paleotectonic and paleoclimatic implications. *Facies*, **60**, 169-194.

Illing, L.V., Wells, A.J. and **Taylor, J.C.M.** (1965) Penecontemporary dolomite in the Persian Gulf. In: *Dolomitization and limestone diagenesis* (Eds L.C. Pray and R.C. Murray), *SEPM Spec. Publ.*, 13, 89-111.

Jones, G.D. and **Xiao, Y.T.** (2005) Dolomitization, anhydrite cementation, and porosity evolution in a reflux system: Insights from reactive transport models. *AAPG Bull.*, **89**, 577-601.

Kaczmarek, S.E. and **Sibley, D.F.** (2011) On the evolution of dolomite stoichiometry and cation order during high-temperature synthesis experiments: An alternative model for the geochemical evolution of natural dolomites. *Sed. Geol.*, **240**, 30-40.

Kocurko, M.J. (1979) Dolomitization by spray-zone brine seepage, San Andres, Colombia. *J. Sed. Petrol.*, **49**, 209-213.

Land, L.S. (1985) The origin of massive dolomite. *J. Geol. Educ.*, **33**, 112-125.

Leary, D.A. and **Vogt, J.N.** (1987) Diagenesis of Permian (Guadalupian) San Andres Formation, Central Basin Platform, West Texas. *AAPG Bull.*, **71**, 582-582.

Logan, B.W. (1987) The MacLeod evaporite basin,Western Australia. *AAPG Memoir*, **44**, 140 p.

Lokier, S.W. (2012) Development and evolution of subaerial halite crust morphologies in a coastal sabkha setting. *J. Arid Environ.*, **79**, 32-47.

Lucia, F.J. (1999) *Carbonate reservoir characterization*. Springer-Verlag, New York, 226 pp.

Lucia, F.J. (2004) Origin and petrophysics of dolostone pore space. In: *The geometry and petrogenesis of dolomite hydrocarbon reservoirs* (Eds C.J.R. Braithwaite, G. Rizzi, and G. Darke), *Geol. Soc. London Spec. Publ.*, 235, 141-155.

Lucia, F.J. and **Major, R.P.** (1994) Porosity evolution through hypersaline reflux dolomitization. In: *Dolomites - A volume in honour of Dolomieu* (Eds B. Purser, M. Tucker., and D. Zenger), *IAS Spec. Publ.*, 21, 325-341.

Lumsden, D.N., Morrison, J.W. and **Lloyd, R.V.** (1995) The role of iron and Mg/Ca ratio in dolomite synthesis at 192°C. *J. Geol.*, **103**, 51-61.

Lüttge, A., Arvidson, R.S. and **Fischer, C.** (2013) A stochastic treatment of crystal dissolution kinetics. *Elements*, **9**, 183-188.

Machel, H.G. (1986) Early lithification, dolomitization, and anhydritization of Upper Devonian Nisku buildups, subsurface of Alberta, Canada. In: *Reef Diagenesis* (Eds J. Schroeder and B. Purser), pp. 336-356. Springer Berlin, Heidelberg.

Machel, H.G. (2004) Concepts and models of dolomitization: a critical reappraisal. In: *The geometry and petrogenesis of dolomite hydrocarbon reservoirs* (Eds C.J.R. Braithwaite, G. Rizzi, and G. Darke), *Geol. Soc. London Spec. Publ.*, 235, 7-63.

Machel, H.G. and Anderson, J.H. (1989) Pervasive subsurface dolomitization of the Nisku Formation in central Alberta. *J. Sed. Res.*, **59**, 891-911.

Machel, H.G. and **Mountjoy, E.W.** (1986) Chemistry and environments of dolomitization - a reappraisal. *Earth-Sci. Rev.*, **23**, 175-222.

Mackenzie, F.T. and **Pigott, J.D.** (1981) Tectonic controls of Phanerozoic sedimentary-rock cycling. *J. Geol. Soc.*, **138,** 183-196.

Martín-Martín, J.D., Gomez-Rivas, E., Bover-Arnal, T., Travé, A., Salas, R., Moreno-Bedmar, J.A., Tomas, S., Corbella, M., Teixell, A., Verges, J. and **Stafford, S.L.** (2013) The Upper Aptian to Lower Albian syn-rift carbonate succession of the southern Maestrat Basin (Spain): Facies architecture and fault-controlled stratabound dolostones. *Cretaceous Res.*, **41**, 217-236.

Mazzullo, S.J. and **Harris, P.M.** (1992) Mesogenetic dissolution: its role in porosity development in carbonate reservoirs. *AAPG Bull.*, **76**, 607-620.

Mazzullo, S.J., Reid, A.M. and **Gregg, J.M.** (1987) Dolomitization of Holocene Mg-calcite supratidal deposits, Ambergris Cay, Belize. *Geol. Soc. Am. Bull.*, **98**, 224-231.

McKenzie, J.A. and **Vasconcelos, C.** (2009) Dolomite Mountains and the origin of the dolomite rock of which they mainly consist: historical developments and new perspectives. *Sedimentology*, **56**, 205-219.

Mehrbach, C., Culberso, C.H., Hawley, J.E. and **Pytkowic, R.M.** (1973) Measurement of apparent dissociation constants of carbonic acid in seawater at atmospheric pressure. *Limnol. Oceanogr.*, **18**, 897-907.

Melim, L.A. and **Scholle, P.A.** (2002) Dolomitization of the Capitan Formation forereef facies (Permian, West Texas and New Mexico): seepage reflux revisited. *Sedimentology*, **49**, 1207-1227.

Montañez, I.P. and **Read, J.F.** (1992) Eustatic control on early dolomitization of cyclic peritidal carbonates: Evidence from the Early Ordovician Upper-Knox Group, Appalachians. *Geol. Soc. Am. Bull*., **104**, 872-886.

Morrow, D.W. (1982) Diagenesis 2. Dolomite - Part 2 Dolomitization models and ancient dolostones. *Geosci. Can.*, **9**, 95-107.

Morse, J.W., Zullig, J.J., Bernstein, L.D., Millero, F.J., Milne, P., Mucci, A. and **Choppin, G.R.** (1985) Chemistry of calcium carbonate rich shallow-water sediments in the Bahamas. *Am. J. Sci.*, **285**, 147-185.

Morse, J.W., Zullig, J.J., Iverson, R.L., Choppin, G.R., Mucci, A. and **Millero, F.J.** (1987) The influence of seagrass beds on carbonate sediments in the Bahamas. *Mar. Chem.*, **22**, 71-83.

Morse, J.W., Wang, Q.W. and **Tsio, M.Y.** (1997) Influences of temperature and Mg:Ca ratio on $CaCO_3$ precipitates from seawater. *Geology*, **25**, 85-87.

Nordstrom, D.K., Plummer, L.N., Wigley, T.M.L., Wolery, T.J., Ball, J.W., Jenne, E.A., Bassett, R.L., Crerar, D.A., Florence, T.M., Fritz, B., Hoffman, M., Holdren, G.R.Jr., Lafon, G.M., Mattigod, S.V., McDuff, R.E., Morel, F., Reddy, M.M., Sposito, G., and **Thrailkill, J.** (1979) A comparison of computerized chemical models for equilibrium calculations in aqueous systems. In: *Chemical modeling in aqueous systems - Speciation, sorption, solubility, and kinetics: Series 93* (Ed E.A. Jenne), American Chemical Society, 857-892.

Palandri, J.L. and **Kharaka, Y.K.** (2004) A compilation of rate parameters of water-mineral interaction kinetics for application to geochemical modeling. U.S. Geological Survey Open File Report 2004-1068.

Palmer, T., Whitaker, F.F., Gabellone, T., Frazer, M.A. and **Garcia-Fresca B.** (2014) Evaluating links between sequence stratigraphy and reflux dolomitisation of the Permian San Andres Formation. In: *AAPG Annual Conference and Exhibition, Search and Discovery Article #90189*, Houston, Texas, 6-9 April.

Pierrot, D., Lewis, E. and **Wallace, D.** (2006) MS Excel Program developed for CO_2 system calculations, Carbon Dioxide Information Analysis Center. Oak Ridge National Laboratory, US Department of Energy, Oak Ridge, TN.

Pogge von Strandmann, P.A.E., Forshaw, J. and **Schmidt, D.N.** (2014) Modern and Cenozoic records of seawater magnesium from foraminiferal Mg isotopes. *Biogeosciences*, **11**, 5155-5168.

Rahimpour-Bonab, H., Esrafili-Dizaji, B. and **Tavakoli, V.** (2010) Dolomitization and anhydrite precipitation in Permo-Triassic carbonates at the South Pars gasfield, offshore Iran: Controls on reservoir quality. *J. Petrol. Geol.*, **33**, 43-66.

Rameil, N. (2008) Early diagenetic dolomitization and dedolomitization of Late Jurassic and earliest Cretaceous platform carbonates: A case study from the Jura Mountains (NW Switzerland, E France). *Sed. Geol.*, **212**, 70-85.

Rivers, J.M., Kyser, T.K. and **James, N.P.** (2012) Salinity reflux and dolomitization of southern Australian slope sediments: the importance of low carbonate saturation levels. *Sedimentology*, **59**, 445-465.

Rott, C.M. and **Qing, H.** (2013) Early dolomitization and recrystallization in shallow marine carbonates, Mississippian Alida Beds, Williston Basin (Canada): Evidence from petrography and isotope geochemistry. *J. Sed. Res.*, **83**, 928-941.

Saller, A.H. (2004) Palaeozoic dolomite reservoirs in the Permian Basin, SW USA: stratigraphic distribution, porosity, permeability and production. In: *The geometry and petrogenesis of dolomite hydrocarbon reservoirs* (Eds C.J.R. Braithwaite, G. Rizzi, and G. Darke), *Geol. Soc. London Spec. Publ.*, 235, 309-324.

Saller, A.H. and **Dickson, J.A.** (2011) Partial dolomitization of a Pennsylvanian limestone buildup by hydrothermal fluids and its effect on reservoir quality and performance: *AAPG Bull.*, **95**, 1745-1762.

Saller, A.H. and **Henderson, N.** (1998) Distribution of porosity and permeability in platform dolomites: Insight from the Permian of West Texas. *AAPG Bull.*, **82**, 1528-1550.

Saller, A.H., Budd, D.A. and **Harris, P.M.** (1994) Unconformities and porosity development in carbonate strata: Ideas from a Hedberg conference. *AAPG Bull.*, **78**, 857-872.

Sandberg, P.A. (1983) An oscillating trend in Phanerozoic non-skeletal carbonate mineralogy. *Nature*, **305**, 19-22.

Sharp, I., Gillespie, P., Morsalnezhad, D., Taberner, C., Karpuz, R., Vergés, J., Horbury, A., Pickard, N., Garland, J. and **Hunt, D.** (2010) Stratigraphic architecture and fracture-controlled dolomitization of the Cretaceous Khami and Bangestan groups: an outcrop case study, Zagros Mountains, Iran. In: *Mesozoic and Cenozoic Carbonate Systems of the Mediterranean and the Middle East: Stratigraphic and Diagenetic Reference Models* (Eds F.S.P. Van Buchem, K.D. Gerdes and M. Esteban), *Geol. Soc. London Spec. Publ.*, 329, 343-396.

Shinn, E.A., Ginsburg, R.N. and **Lloyd, R.M.** (1965) Recent supratidal dolomite from Andros Island, Bahamas. In: *Dolomitization and limestone diagenesis* (Eds L.C. Pray and R.C. Murray), *SEPM Spec. Publ.*, 13, 112-123.

Sibley, D.F., Dedoes, R.E. and **Bartlett, T.R.** (1987) Kinetics of dolomitization. *Geology*, **15**, 1112-1114.

Sibley, D.F., Nordeng, S.H. and **Borkowski, M.L.** (1994) Dolomitization kinetics in hydrothermal bombs and natural settings. *J. Sed. Res.*, **A64**, 630-637.

Simms, M. (1984) Dolomitization by groundwater-flow systems in carbonate platforms. *Trans. Gulf Coast Assoc. Geol. Soc.*, **34**, 411-420.

Smith, L.B.J., Eberli , G.P. and **Sonnenfeld, M.** (2004) Sequence-stratigraphic and paleogeographic distribution of reservoir-quality dolomite, Madison Formation, Wyoming and Montana. In: *Integration of outcrop and modern analogs in reservoir modeling* (Eds G.M. Grammer, P.M. Harris and G.P. Eberli), *AAPG Memoir*, 80, 67– 92.

Sonnenfeld, M. (1996) Sequence evolution and hierarchy within the Lower Mississippian Madison limestone of Wyoming. In: *Paleozoic Systems of the Rocky Mountain Region* (Eds M.W. Longman and M.D. Sonnenfeld), *Rocky Mountain Section, SEPM*, 165-192.

Steuber, T. and **Rauch, M.** (2005) Evolution of the Mg/Ca ratio of Cretaceous seawater: Implications from the composition of biological low-Mg calcite. *Mar. Geol.*, **217**, 199-213.

Sun, S.Q. (1994) A reappraisal of dolomite abundance and occurrence in the Phanerozoic. *J. Sed. Res.*, **A64**, 396-404.

Sun, S.Q. (1995) Dolomite reservoirs - porosity evolution and reservoir characteristics. *AAPG Bull.*, **79**, 186-204.

Swart, P.K. and **Melim, L.A.** (2000) The origin of dolomites in tertiary sediments from the margin of Great Bahama Bank. *J. Sed. Res.*, **70**, 738-748.

Timofeeff, M.N., Lowenstein, T.K., da Silva, M.A. and **Harris, N.B.** (2006) Secular variation in the major-ion chemistry of seawater: Evidence from fluid inclusions in Cretaceous halites. *Geochim. Cosmochim. Acta*, **70**, 1977-1994.

Vandeginste, V., John, C.M. and **Manning, C.** (2013) Interplay between depositional facies, diagenesis and early fractures in the Early Cretaceous Habshan Formation, Jebel Madar, Oman. *Mar. Petrol. Geol.*, **43**, 489-503.

Vasconcelos, C. and **McKenzie, J.A.** (1997) Microbial mediation of modern dolomite precipitation and diagenesis under anoxic conditions (Lagoa Vermelha, Rio de Janeiro, Brazil). *J. Sed. Res.*, **67**, 378-390.

Wahlman, G.P. (2010) Reflux dolomite crystal size variation in cyclic inner ramp reservoir facies, Bromide Formation (Ordovician), Arkoma Basin, Southeastern Oklahoma. *The Sedimentary Record*, **8**, 4-9.

Walter, L.M. and **Burton, E.A.** (1990) Dissolution of recent platform carbonate sediments in marine pore fluids. *Am. J. Sci.*, **290**, 601-643.

Warren, J. (2000) Dolomite: occurrence, evolution and economically important associations. *Earth-Sci. Rev.*, **52**, 1-81.

Whitaker, F.F. and **Smart, P.L.** (1990) Active circulation of saline ground waters in carbonate platforms: Evidence from the Great Bahama Bank. *Geology*, **18,** 200-203.

Whitaker, F.F. and **Xiao, Y.** (2010) Reactive transport modeling of early burial dolomitization of carbonate platforms by geothermal convection. *AAPG Bull.*, **94**, 889-917.

Whitaker, F.F., Ooi S.M.D., Jameson J. and **Strohmenger C.** (2014) Origins of evaporites in a Holocene mixed clastic and carbonate coastal sabkha: Preliminary hydrological and geochemical data from Mesaieed sabkha, Qatar. *IPTC* 17567.

Wilkinson, B.H. and **Algeo, T.J.** (1989) Sedimentary carbonate record of calcium-magnesium cycling. *Am. J. Sci.*, **289**, 1158-1194.

Wilson, A.M., Sanford, V., Whitaker, F. and **Smart, P.** (2001) Spatial patterns of diagenesis during geothermal circulation in carbonate platforms. *Am. J. Sci.*, **301,** 727-752.

Wolery, T.J. (1992) EQ3/EQ6, a software package for geochemical modeling of aqueous systems, package overview and installation guide (version 7.0). Lawrence Livermore National Laboratory Report UCRL-MA-110662(1).

Woody, R.E., Gregg, J.M. and **Koederitz, L.F.** (1996) Effect of texture on petrophysical properties of dolomite: Evidence from the Cambrian-Ordovician of southeastern Missouri. *AAPG Bull.*, **80**, 119-132.

Wright, P. and **Harris, P.M.** (2013) Carbonate dissolution and porosity development in the burial (mesogenetic) environment. In: *AAPG Annual Convention and Exhibition, Search and Discovery Article #50860*, Pittsburgh, Pennsylvania, 19-22 May.

Xu, T.F., Sonnenthal, E., Spycher, N. and **Pruess, K.** (2004) TOUGHREACT user's guide: A simulation program for non-isothermal multiphase reactive geochemical transport in variable saturated geologic media. Lawrence Berkeley National Laboratory Report LBNL-55460, Berkeley, California.

Xu, T.F., Apps, J.A. and **Pruess, K.** (2005) Mineral sequestration of carbon dioxide in a sandstone-shale system. *Chem. Geol.*, **217**, 295-318.

Zeebe, R.E. (2012) History of seawater carbonate chemistry, atmospheric CO_2, and ocean acidification. *Annu. Rev. Earth Planet. Sci.*, **40**, 141-165.

Table and Figure Captions

Table 1: Aqueous species included in the reactive transport simulations.

Table 2: Chemical composition of initial seawaters at 30 °C and atmospheric pCO_2 used in 1D simulations of reflux. Modern seawater composition from Nordstrom *et al.* (1979); Aptian seawater composition from Timofeeff *et al.*, (2006); and Mississippian seawater composition from Demicco *et al.* (2005).

Figure 1: Saturation indices of simulated carbonate and sulphate minerals during evaporation of modern (A), Aptian (B) and Mississippian (C) seawater at 30 °C.

Figure 2: Volume of dolomite precipitated from different normal marine (35‰) seawaters at 30 °C from three different times in closed system (batch) reactive transport simulations.

Figure 3: Changes in mineralogy (volume fraction; A-C, E and F) and percent porosity (D) over 500 kyr predicted by reactive transport simulations of 30 °C modern normal-marine seawater and seawater-derived brines at 9.5 m depth. Mass-balance calculations allow discrimination between replacive dolomite (C) and dolomite cement (E). The upper x-axis in A and B represents the time relative to that required for complete replacement of calcite by dolomite by normal modern seawater (1).

Figure 4: Reactive transport modelling results for 30 °C modern and Mississippian normal-marine seawaters and seawater-derived brines at 9.5 m depth. A) Time required to dolomitise all the initial calcite. For both modern and Mississippian fluids the time needed to replace calcite has an inverse power-law correlation to salinity. Dolomitisation time increases substantially for the 200‰ Mississippian brine due to gypsum precipitation which occludes pore volume and reduces flow rates. B) Porosity loss at 100 kyr after complete calcite replacement. Porosity reduction is due to dolomite cementation and shows a linear correlation with salinity for both modern and Mississippian fluids below gypsum saturation.

Figure 5: Changes in mineralogy (volume fraction; A-C, E and F) and percent porosity (D) over 500 kyr as predicted by reactive transport simulations of 30 °C Mississippian (solid

lines) and Aptian (dashed lines) seawaters and seawater-derived brines at 9.5 m depth. Mass-balance calculations allowed discrimination between replacive dolomite (C) and dolomite cement (E) for the Mississippian fluids. The simultaneous precipitation of calcite and dolomite from Aptian fluids prohibits these calculations. For the 200‰ brines, only the gypsum volume fraction is displayed (F).

Figure 6: Reactive transport modelling results for (A) modern and (B) Mississippian seawaters and their associated seawater-derived brines at 30 °C as a function of precursor mineralogy (calcite or aragonite). The time required to dolomitise all the initial $CaCO_3$ is displayed at 9.5 m depth and shows an inverse power-law correlation with brine salinity, with the exception of the 200‰ Mississippian brine for which dolomitisation is slowed as a result of gypsum precipitation occluding pore volume and reducing fluid fluxes.

Figure 7: Changes in mineralogy (volume fraction; A-C) and percent porosity (D) for simulations using different kinetic rate constants for both aragonite and calcite. Results are for reflux of 30 °C Mississippian seawater-derived brine of 89‰ salinity at 9.5 m. Enlargement in C shows the loss of aragonite over the first 10 kyr.

Figure 8: Changes in mineralogy (volume fraction; A-D) and percent porosity (E) for Mississippian seawater-derived brines of 89‰ salinity at different temperatures and at 9.5 m depth. F) Time to dolomitise all calcite and extent of porosity loss 100 kyr after complete calcite replacement. Note the negative power-law relationship between time needed to complete replacement and temperature and the linear relationship between porosity loss and temperature.

Figure 9: Changes in mineralogy (volume fraction; A-D) and percent porosity (E) for Mississippian brine of 89‰ salinity in equilibrium with different pCO_2 values at 9.5 m depth. F) Time to dolomitise all calcite and porosity loss 100 kyr after complete calcite replacement. Note the negative logarithmic relationship between the time to complete replacement and pCO_2. For pCO_2 of 350 and 1000 ppmv, simultaneous calcite and dolomite precipitation hinders discrimination of cement and replacement dolomite volumes.

Figure 10: Changes in mineralogy (volume fraction; A-D) and percent porosity (E) for different reactive surface areas (RSA) and Mississippian brine of 89‰ salinity. Data from 9.5 m depth. F) Time to dolomitise all calcite and porosity loss 100 kyr after complete calcite replacement at 9.5 m depth. Note the negative power-law and logarithmic relationships between the time to complete replacement and RSA and between porosity loss and RSA, respectively. For RSA = 100 and 250 cm^2/g, the simultaneous occurrence of calcite and dolomite precipitation prohibits calculation of cement and replacement dolomite volumes.

Figure 11: Depth distribution of total dolomite (A), replacive dolomite (B), and dolomite cement (C) formed by injection of 89‰ Mississippian brine at rates from 0.01 to 2 m/yr, plotted for 100 kyr (dashed lines) and 500 kyr (solid lines). Note for figure B that replacement is complete in all simulations at 500 kyr.

Figure 12: Changes in mineralogy (volume fraction; A-D) and percent porosity (E) for different injection rates of Mississippian brine of 89‰. F) Time required to dolomitise all calcite and porosity loss 100 kyr after complete calcite replacement at 9.5 m depth. Note the negative power-law and the logarithmic relationships between time to complete replacement and fluid flux and between porosity loss and fluid flux, respectively.

Figure 13: A) Relationship between brine salinity for fluids below gypsum saturation and the exponent *x* of the equation $Dol_t = Dol_0 e^{(xt)}$ describing the rate of dolomite formation, where Dol_t is dolomite volume fraction at time *t*, Dol_0 is the initial ("seed") dolomite volume fraction, and *t* is the time in kyr. For each source water the exponent is a product of the salinity and a gradient term *a* (R^2 for all three fluids >0.99). B) Relationship between the Mg/Ca molar ratio of the source fluids and the gradient *a* of each of the best fit lines of Figure 13A; $y=5.934E\text{-}8x^{1.847}$.

Figure 14: Secular changes of seawater Mg/Ca molar ratio from Hardie (1996; A); percentage of replacive dolomite predicted from normal marine seawater and two evaporative brines in 100 kyr assuming 1% of dolomite "seed" and 40% porosity using equation 2 (B); and dolomite abundance as percent of the total carbonate rock record from Given & Wilkinson (1987; C).

Figure 15: Tornado diagrams summarising the sensitivity analysis of 1D reactive transport simulations using 89‰ Mississippian brine at 30 °C as the baseline. Results are displayed at 9.5 m depth. The baseline simulation is represented by the black vertical line, whist the length of the horizontal bars shows the range of replacement times (A) and the range of volumes of dolomite cement precipitated 100 kyr after replacement (B) spanned by simulations over the specified range of parameter values. Curves drawn inside each bar represent the form of the relationship (power-law, logarithmic, linear; positive or negative) between each controlling parameter and the diagenetic response.

Captions of online supplementary figures:

Figure S1: Changes in mineralogy (volume fraction; A-C, E and F) and percent porosity (D) over 500 kyr as predicted by reactive transport simulations of 30 °C Mississippian seawater and seawater-derived brines at 9.5 m depth. Mass-balance calculations allowed discrimination between replacive dolomite (C) and dolomite cement (E).

Figure S2: Changes in mineralogy (volume fraction; A-C) and percent porosity (D) over 500 kyr as predicted by reactive transport simulations of 30 °C Aptian seawater and seawater derived brines at 9.5 m depth. The simultaneous precipitation of calcite and dolomite prohibits calculation of replacive and cement dolomite volumes.

Primary Acqueous Species					
H_2O	H^+	Ca^{2+}	Mg^{2+}	Na^+	K^+
HCO_3^-	SO_4^{2-}	Cl^-			
Secondary Acqueous Species					
$CaCO_3(aq)$	$CaHCO_3^+$	$CaOH^+$	$CaSO_4(aq)$	$CO_2(aq)$	CO_3^{2-}
$HSO4^-$	$MgCO_3(aq)$	$MgHCO_3^+$	$MgOH^+$	OH^-	

Component (mol/Kg)	Modern seawater	Aptian seawater	Early Carboniferous seawater
pH	8.22	7.6	7.7
Na^{+}	$4.85e^{-1}$	$4.15e^{-1}$	$4.77e^{-1}$
Mg^{2+}	$5.51e^{-2}$	$4.20e^{-2}$	$4.46e^{-2}$
Ca^{2+}	$1.07e^{-2}$	$3.55e^{-2}$	$1.93e^{-2}$
K^{+}	$1.06e^{-2}$	$1.10e^{-2}$	$1.12e^{-2}$
Cl^{-}	$5.66e^{-1}$	$5.65e^{-1}$	$5.76e^{-1}$
SO_4^{-2}	$2.93e^{-2}$	$8.50e^{-3}$	$1.83e^{-2}$
HCO_3^{-}	$2.13e^{-3}$	$2.92e^{-3}$	$3.14e^{-3}$
pCO_2(ppmv)	394	2400	1400
Mg/Ca molar ratio	5.1	1.2	2.3
Saturation index			
Dolomite	3.51	3.08	3.07
Calcite	0.78	0.87	0.73
Gypsum	-0.77	-0.76	-0.70
Anhydrite	-0.89	-0.87	-0.81

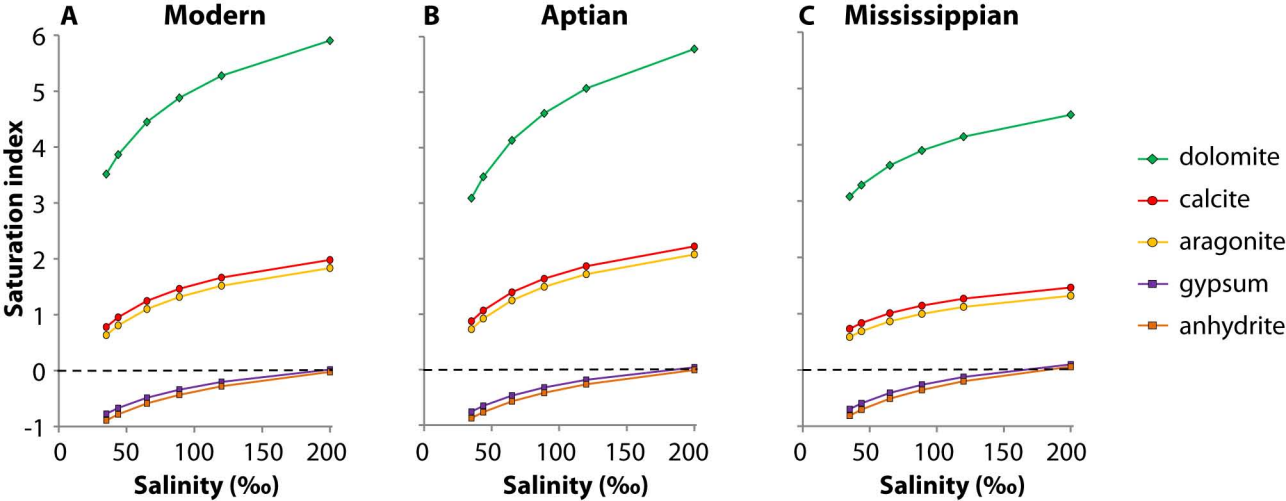
A
Modern
B
Aptian
C
Mississippian
Saturation index
6
5
4
3
2
1
0
-1
0
50
100
150
200
Salinity (‰)
dolomite
calcite
aragonite
gypsum
anhydrite

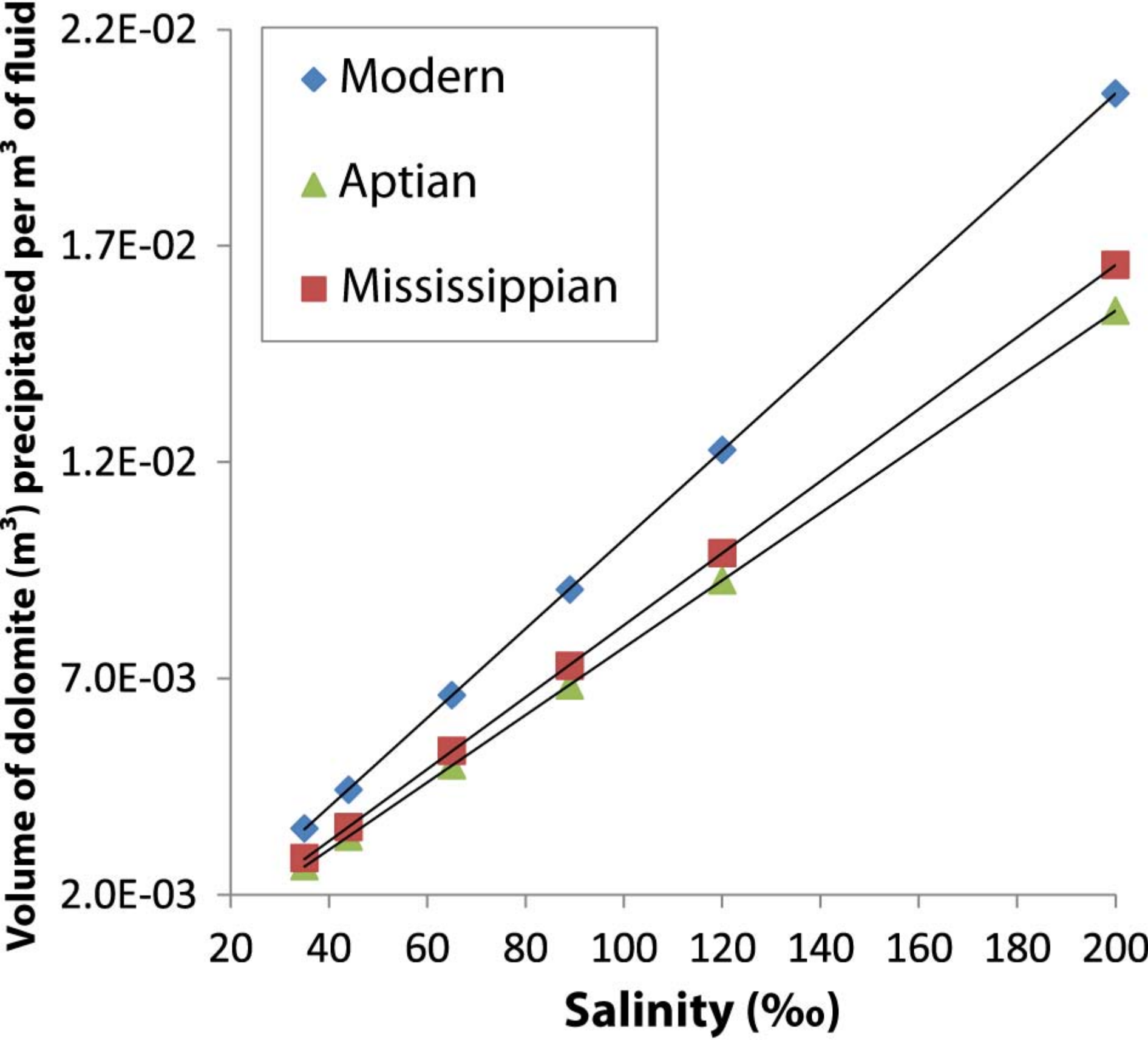
Modern
Aptian
Mississippian
2.2E-02
1.7E-02
1.2E-02
7.0E-03
2.0E-03
Volume of dolomite (m3) precipitated per m3 of fluid
20
40
60
80
100
120
140
160
180
200
Salinity (‰)

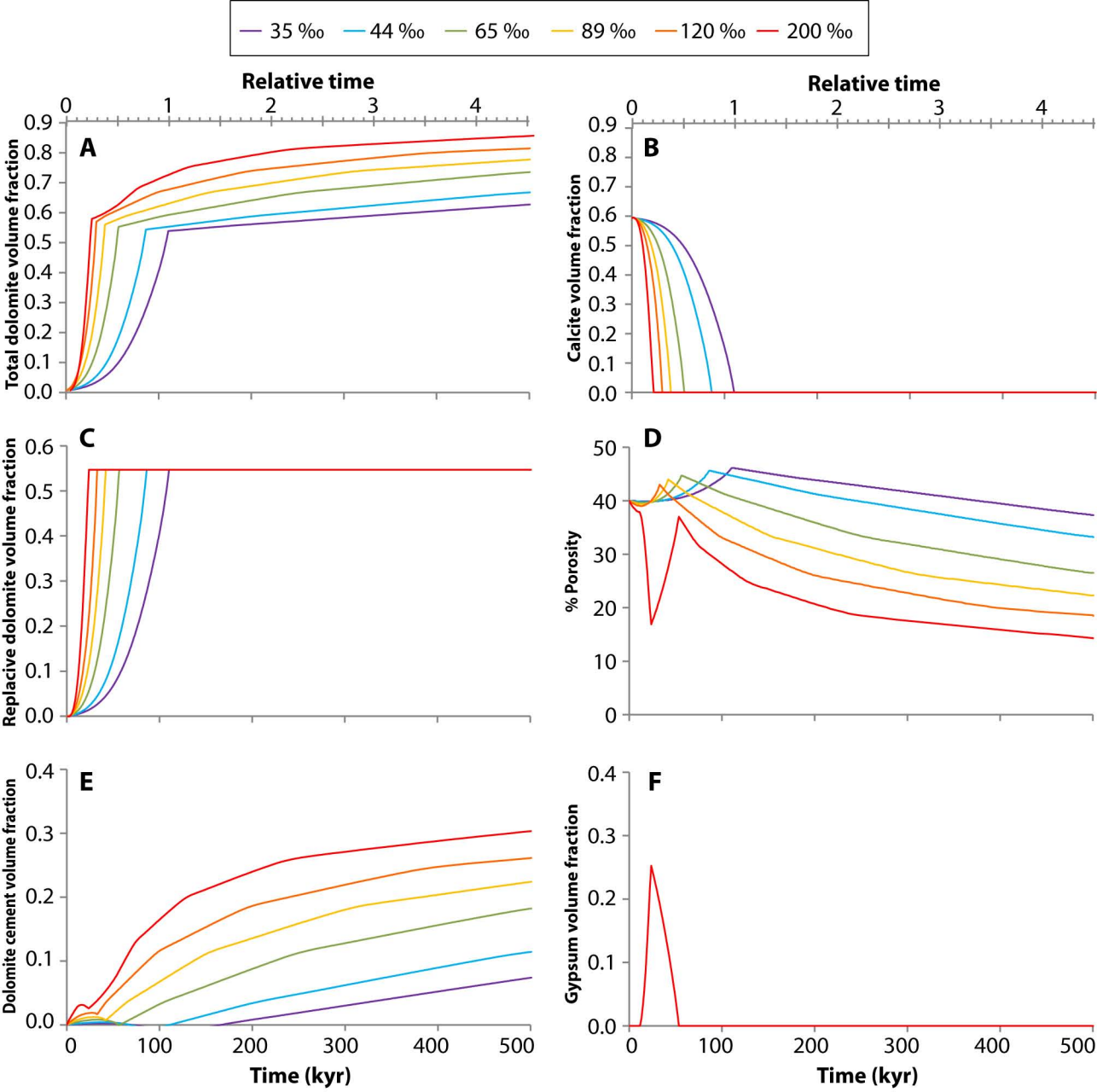
35 ‰
44 ‰
65 ‰
89 ‰
120 ‰
200 ‰
Relative time
A
Total dolomite volume fraction
B
Calcite volume fraction
C
Replacive dolomite volume fraction
D
% Porosity
E
Dolomite cement volume fraction
F
Gypsum volume fraction
Time (kyr)

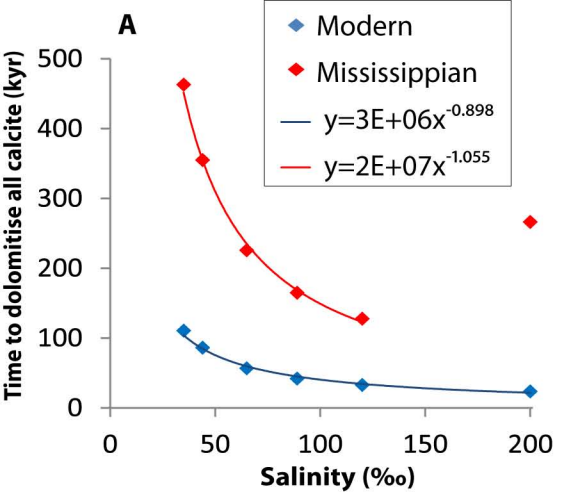
A
Modern
Mississippian
y=3E+06x-0.898
y=2E+07x-1.055
Time to dolomitise all calcite (kyr)
500
400
300
200
100
0
0
50
100
150
200
Salinity (‰)

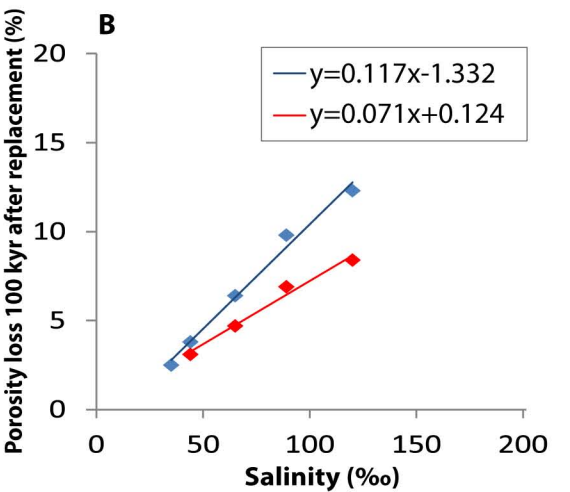
B
y=0.117x-1.332
y=0.071x+0.124
Porosity loss 100 kyr after replacement (%)
20
15
10
5
0
0
50
100
150
200
Salinity (‰)

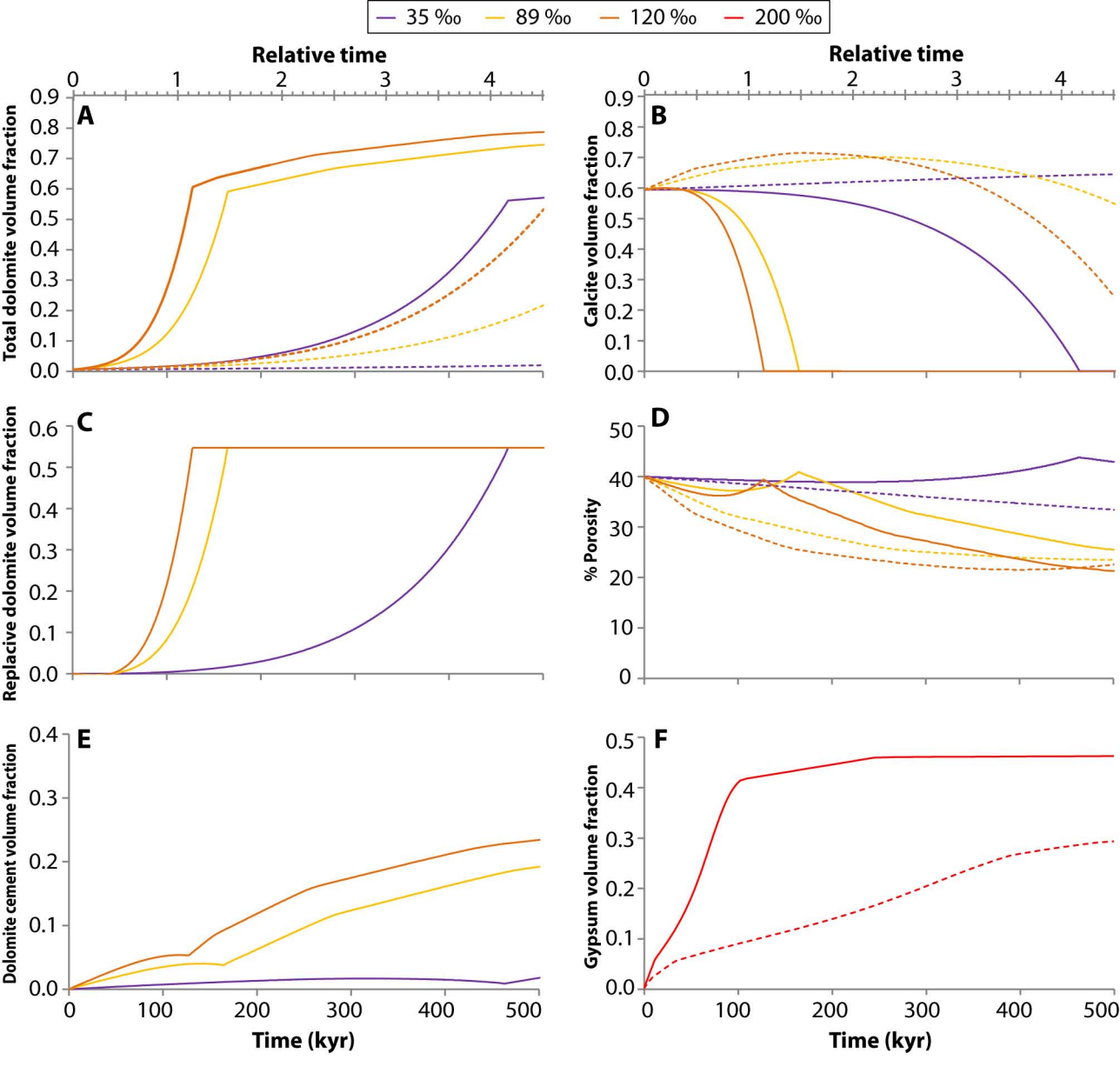
35 ‰
89 ‰
120 ‰
200 ‰
Relative time
A
Total dolomite volume fraction
B
Calcite volume fraction
C
Replacive dolomite volume fraction
D
% Porosity
E
Dolomite cement volume fraction
F
Gypsum volume fraction
Time (kyr)
Time (kyr)

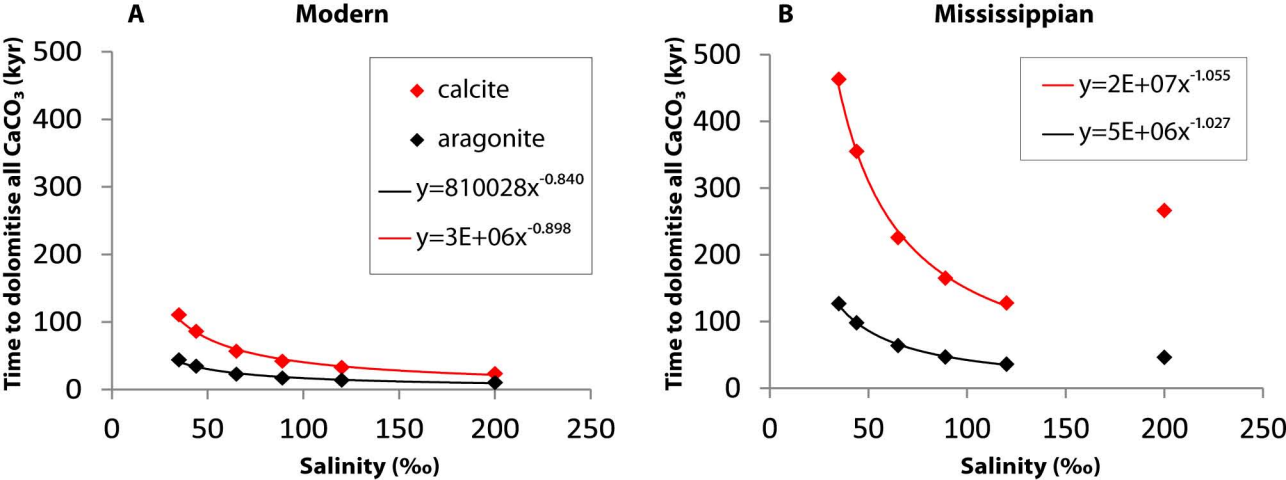
A
Modern
B
Mississippian
Time to dolomitise all CaCO3 (kyr)
Salinity (‰)
calcite
aragonite
y=810028x-0.840
y=3E+06x-0.898
y=2E+07x-1.055
y=5E+06x-1.027
0
100
200
300
400
500
50
150
250

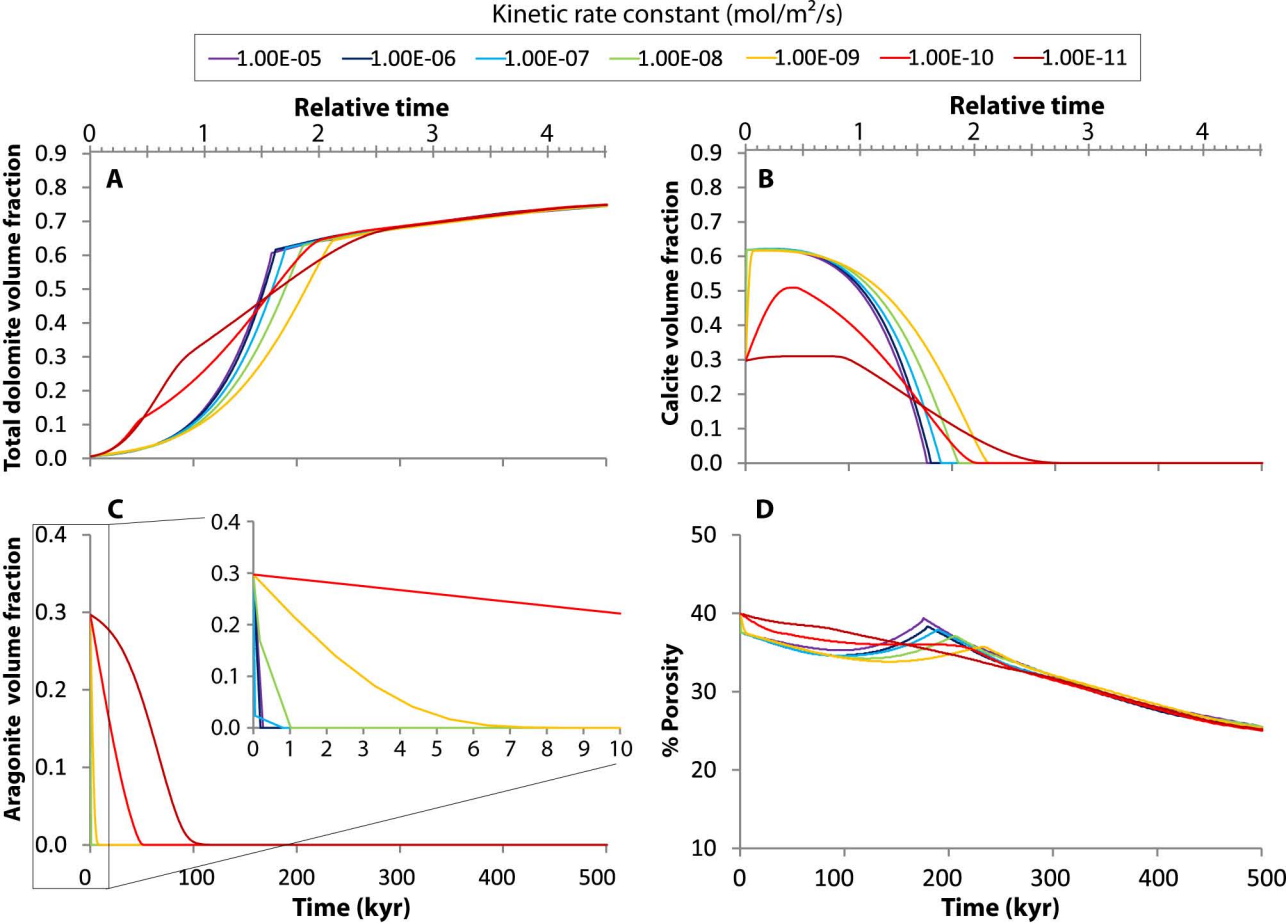
Kinetic rate constant (mol/m²/s)
1.00E-05
1.00E-06
1.00E-07
1.00E-08
1.00E-09
1.00E-10
1.00E-11
Relative time
A
Total dolomite volume fraction
B
Calcite volume fraction
C
Aragonite volume fraction
Time (kyr)
D
% Porosity
Time (kyr)

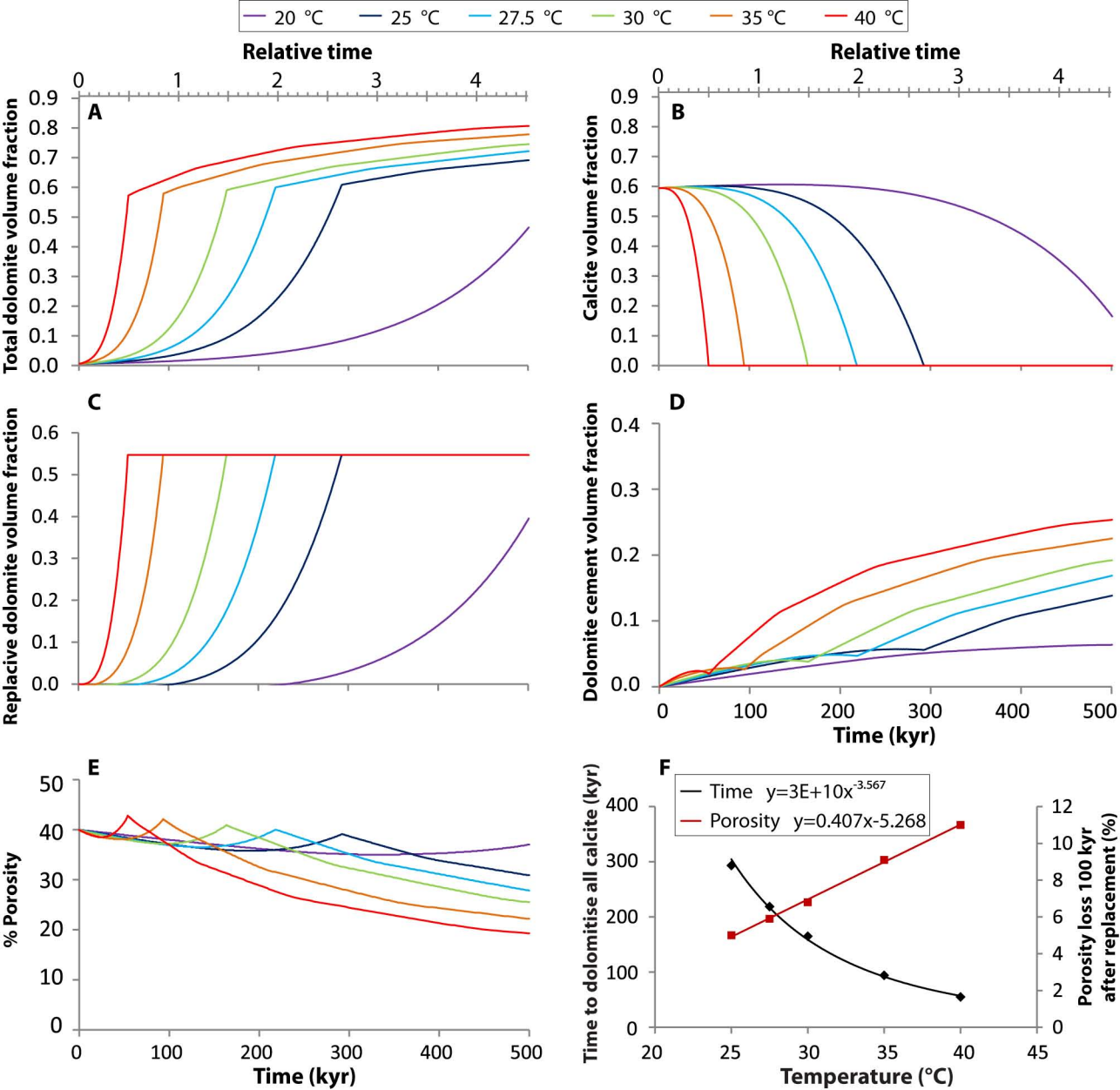
20 °C
25 °C
27.5 °C
30 °C
35 °C
40 °C
Relative time
A
Total dolomite volume fraction
B
Calcite volume fraction
C
Replacive dolomite volume fraction
D
Dolomite cement volume fraction
Time (kyr)
E
% Porosity
Time (kyr)
F
Time y=3E+10x^-3.567
Porosity y=0.407x-5.268
Time to dolomitise all calcite (kyr)
Porosity loss 100 kyr after replacement (%)
Temperature (°C)

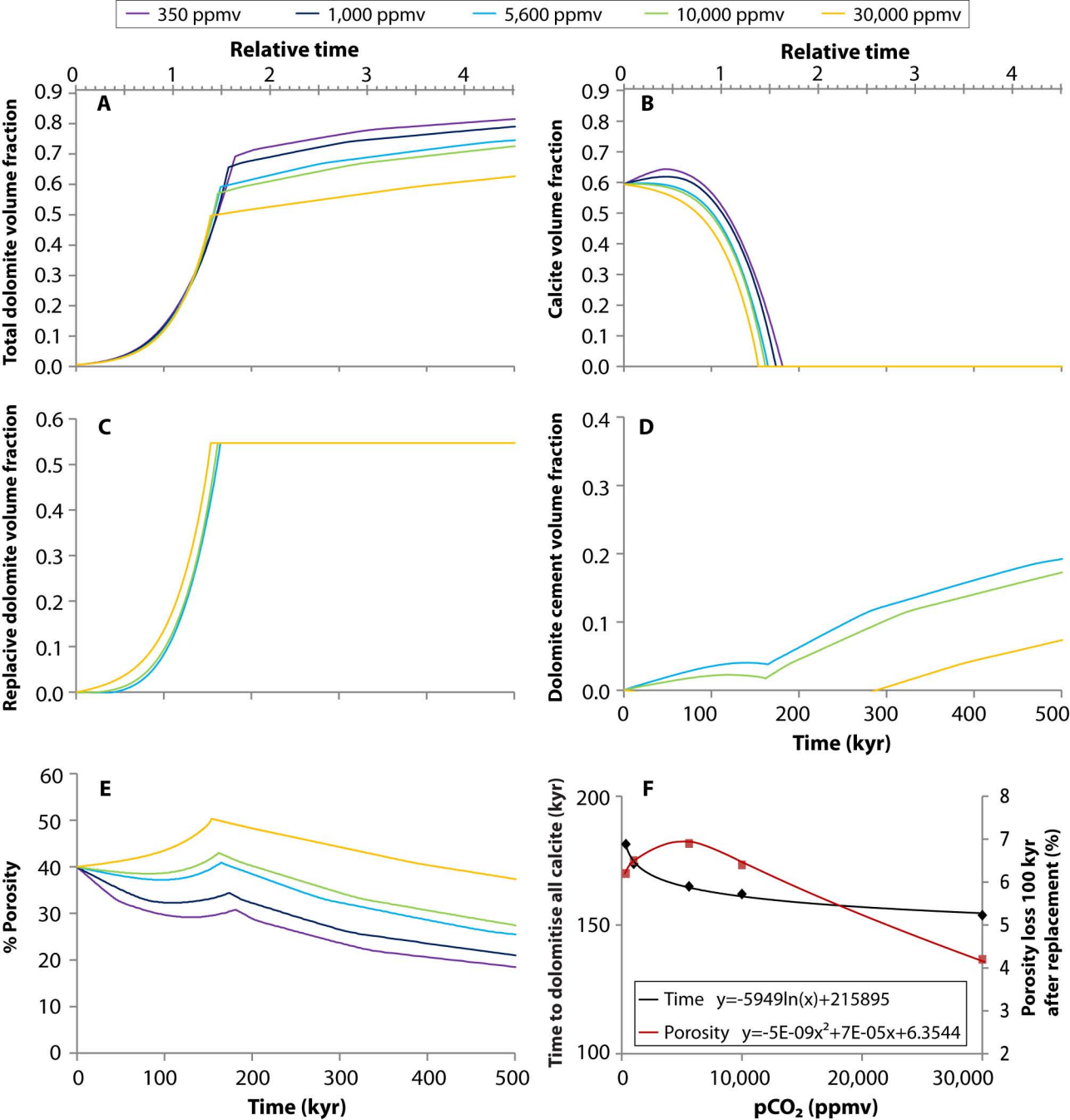
350 ppmv
1,000 ppmv
5,600 ppmv
10,000 ppmv
30,000 ppmv
Relative time
A
Total dolomite volume fraction
B
Calcite volume fraction
C
Replacive dolomite volume fraction
D
Dolomite cement volume fraction
Time (kyr)
E
% Porosity
Time (kyr)
F
Time to dolomitise all calcite (kyr)
Porosity loss 100 kyr after replacement (%)
Time y=-5949ln(x)+215895
Porosity y=-5E-09x²+7E-05x+6.3544
pCO₂ (ppmv)

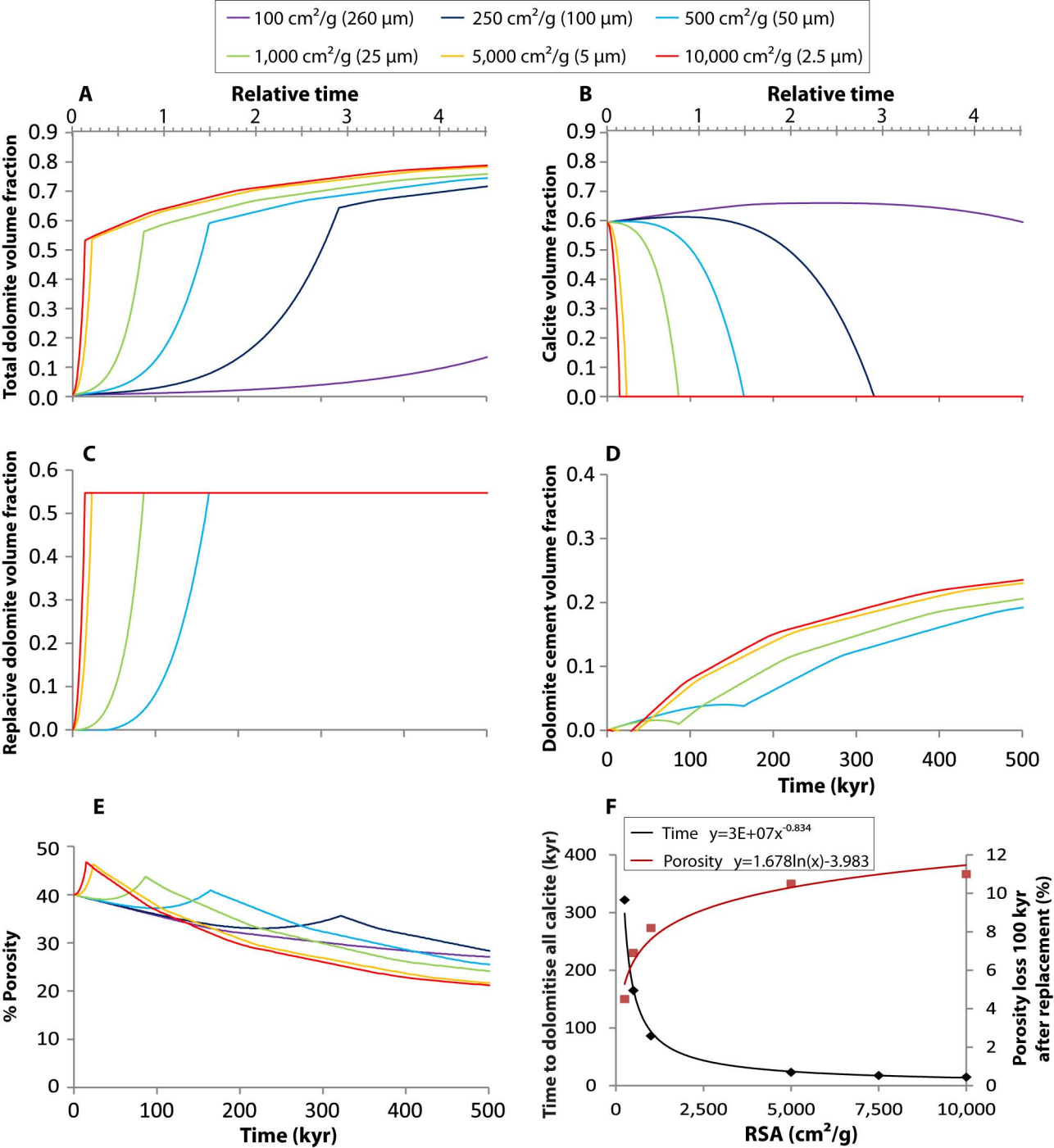
100 cm²/g (260 µm)
250 cm²/g (100 µm)
500 cm²/g (50 µm)
1,000 cm²/g (25 µm)
5,000 cm²/g (5 µm)
10,000 cm²/g (2.5 µm)
A
Relative time
Total dolomite volume fraction
B
Relative time
Calcite volume fraction
C
Replacive dolomite volume fraction
D
Dolomite cement volume fraction
Time (kyr)
E
% Porosity
Time (kyr)
F
Time y=3E+07x^-0.834
Porosity y=1.678ln(x)-3.983
Time to dolomitise all calcite (kyr)
Porosity loss 100 kyr after replacement (%)
RSA (cm²/g)

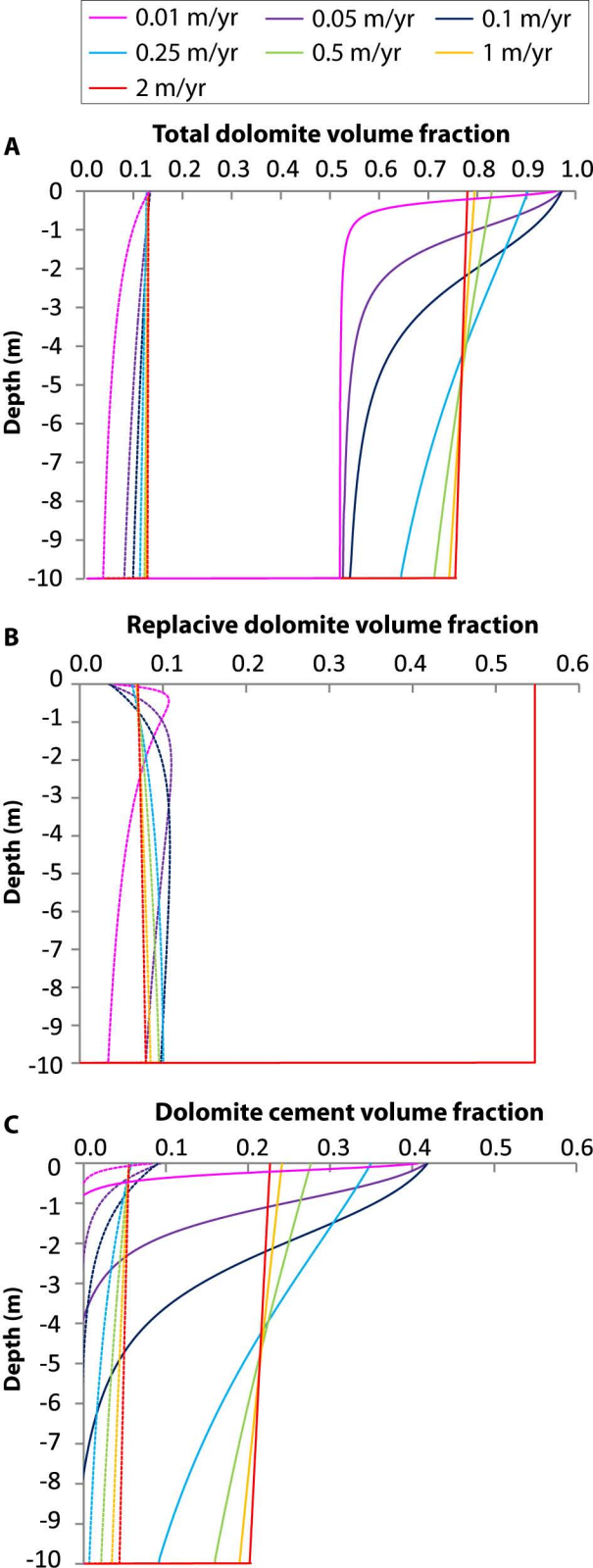
0.01 m/yr
0.05 m/yr
0.1 m/yr
0.25 m/yr
0.5 m/yr
1 m/yr
2 m/yr
A
Total dolomite volume fraction
0.0 0.1 0.2 0.3 0.4 0.5 0.6 0.7 0.8 0.9 1.0
0 -1 -2 -3 -4 -5 -6 -7 -8 -9 -10
Depth (m)
B
Replacive dolomite volume fraction
0.0 0.1 0.2 0.3 0.4 0.5 0.6
0 -1 -2 -3 -4 -5 -6 -7 -8 -9 -10
Depth (m)
C
Dolomite cement volume fraction
0.0 0.1 0.2 0.3 0.4 0.5 0.6
0 -1 -2 -3 -4 -5 -6 -7 -8 -9 -10
Depth (m)

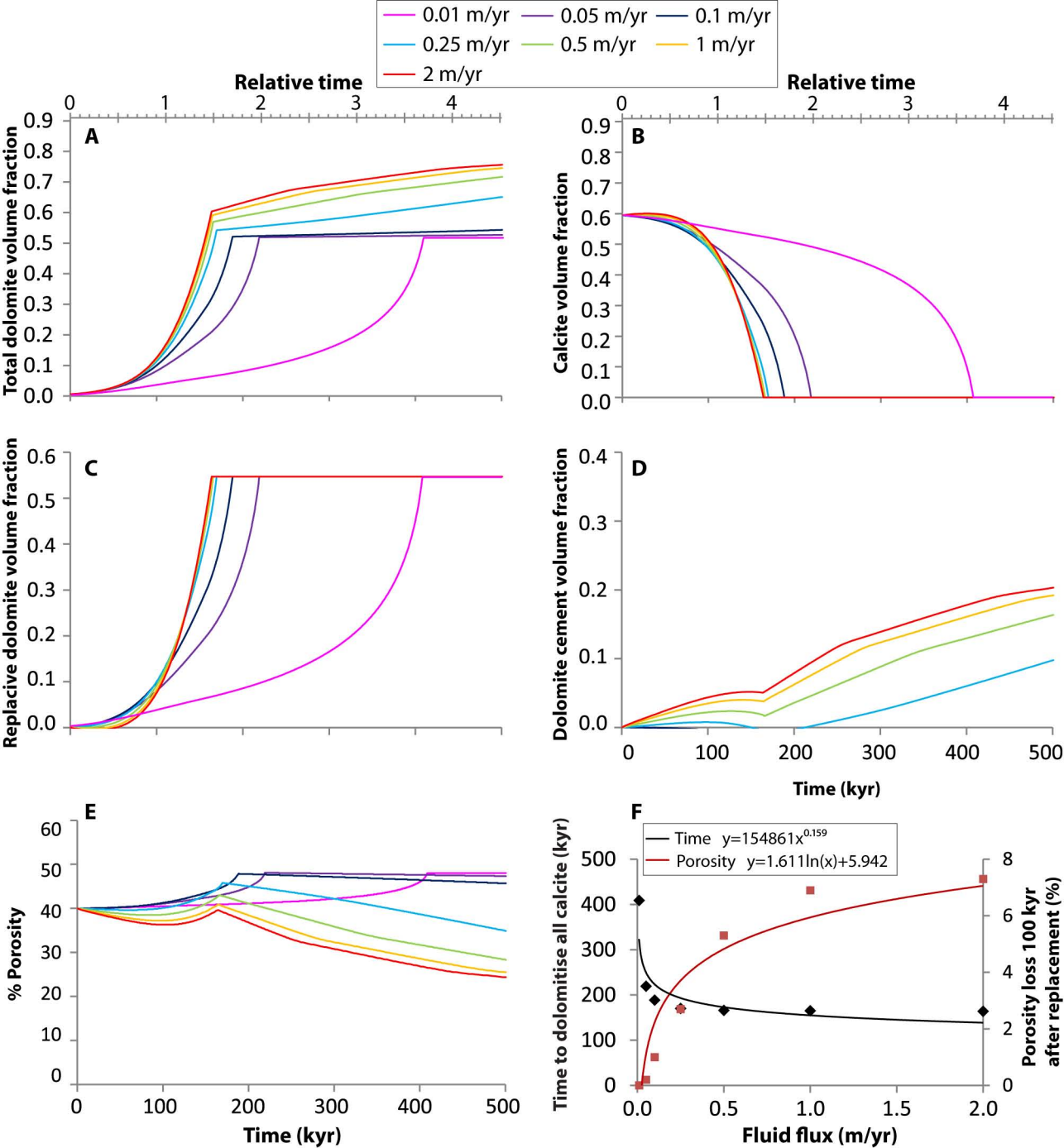
0.01 m/yr
0.05 m/yr
0.1 m/yr
0.25 m/yr
0.5 m/yr
1 m/yr
2 m/yr
Relative time
A
Total dolomite volume fraction
B
Calcite volume fraction
C
Replacive dolomite volume fraction
D
Dolomite cement volume fraction
Time (kyr)
E
% Porosity
Time (kyr)
F
Time y=154861x^0.159
Porosity y=1.611ln(x)+5.942
Time to dolomitise all calcite (kyr)
Porosity loss 100 kyr after replacement (%)
Fluid flux (m/yr)

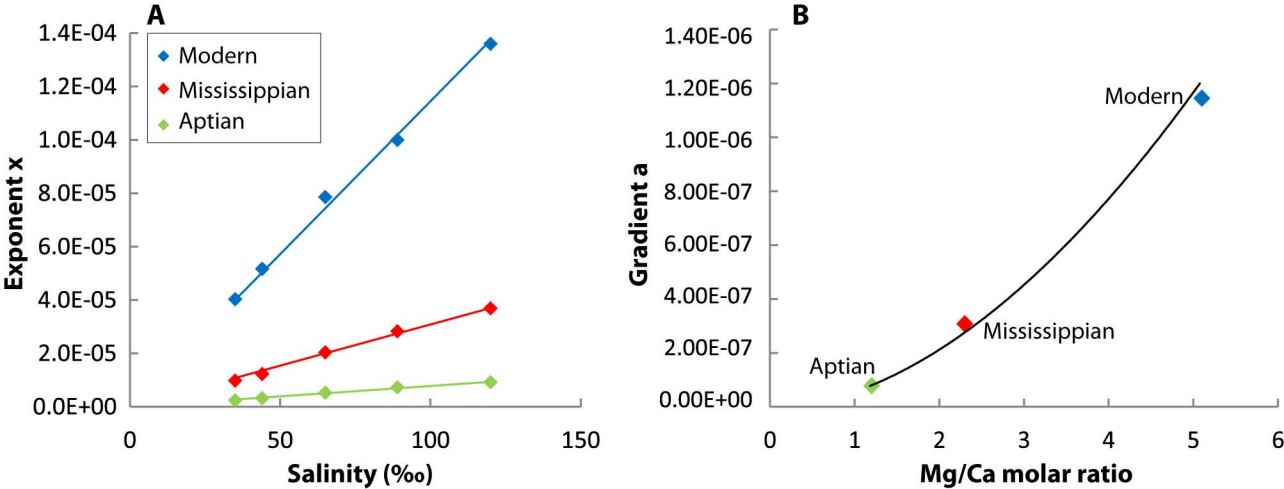
A
Modern
Mississippian
Aptian
Exponent x
1.4E-04
1.2E-04
1.0E-04
8.0E-05
6.0E-05
4.0E-05
2.0E-05
0.0E+00
0
50
100
150
Salinity (‰)
B
Gradient a
1.40E-06
1.20E-06
1.00E-06
8.00E-07
6.00E-07
4.00E-07
2.00E-07
0.00E+00
Modern
Mississippian
Aptian
0
1
2
3
4
5
6
Mg/Ca molar ratio

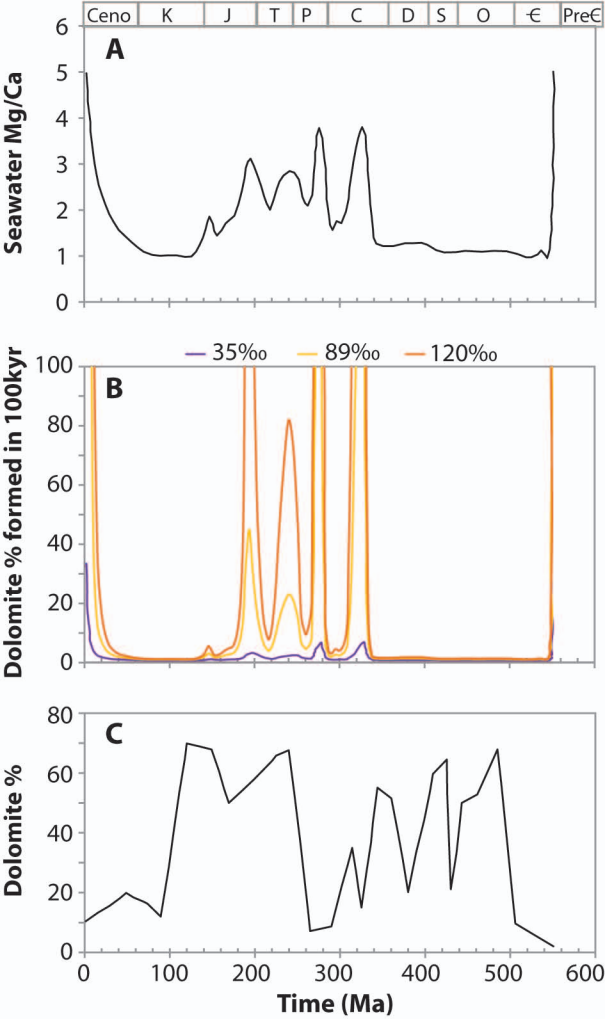
Ceno
K
J
T
P
C
D
S
O
Є
PreЄ
A
Seawater Mg/Ca
6
5
4
3
2
1
0
35‰
89‰
120‰
B
Dolomite % formed in 100kyr
100
80
60
40
20
0
C
Dolomite %
80
60
40
20
0
0
100
200
300
400
500
600
Time (Ma)

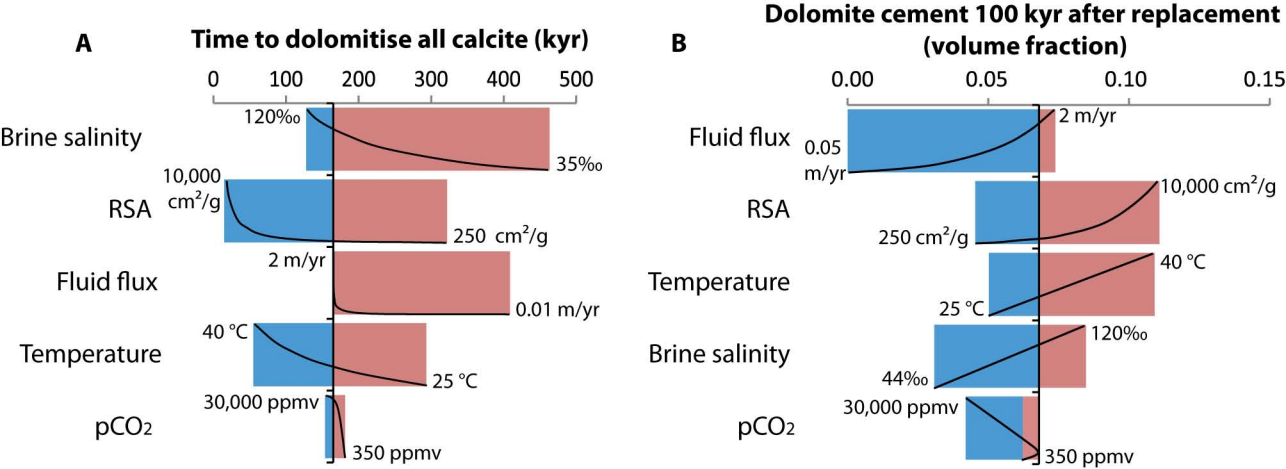
A
Time to dolomitise all calcite (kyr)
0
100
200
300
400
500
Brine salinity
120‰
35‰
RSA
10,000 cm²/g
250 cm²/g
Fluid flux
2 m/yr
0.01 m/yr
Temperature
40 °C
25 °C
pCO2
30,000 ppmv
350 ppmv
B
Dolomite cement 100 kyr after replacement (volume fraction)
0.00
0.05
0.10
0.15
Fluid flux
0.05 m/yr
2 m/yr
RSA
250 cm²/g
10,000 cm²/g
Temperature
25 °C
40 °C
Brine salinity
44‰
120‰
pCO2
30,000 ppmv
350 ppmv